PLANETARY PHYSICS III:
PHOTOIONIZATION CROSS SECTIONS OF THE RARE GASES

J. A. R. Samson and F. L. Kelly

January 1964 74 p refer

(NASA Contract No. NASw-840)

Prepared for

National Aeronautics and Space Administration
Headquarters
Washington, D. C. 20546

GEOPHYSICS CORPORATION OF AMERICA
Bedford, Massachusetts 01730

TABLE OF CONTENTS

LIST OF FIGURES

LIST OF TABLES

PHOTOIONIZATION CROSS SECTIONS OF THE RARE GASES

J.A.R. Samson and F.L. Kelley

I. INTRODUCTION

The interaction of radiation of wavelengths shorter than 1000 Å with a gas will in general produce ionization in the gas. The cross section for the ionizing process is an important parameter in many fields of science. For example, the extreme ultraviolet radiation from the sun interacts with the earth's atmosphere creating the ionosphere, the various layers of which are produced by different regions of the extreme UV even extending down to the x-ray region. Other examples can be found in gaseous discharges including thermo-nuclear devices. Here radiation created by the discharge can be reabsorbed by the neutral and ionized atoms. Any serious investigation of such devices must include knowledge of the photoionization cross section of the gases involved. In the theoretical field experimental data are required to check the validity of the various models for the photoionization process. This is extremely important since in many cases, e.g., atomic oxygen and hydrogen, experimental data is unavailable and one must rely on theoretical values.

This present investigation was motivated largely to provide a check for the available theoretical models. The rare gases were used since they are normally in an atomic state and hence the interpretation of their absorption spectrum was easier. Further, some theoretical work has been performed on them and is available for comparison with experimental work. Another important motivation is that the rare gases are

used as absolute standards in determining the intensity of radiation below 1000 Å and for the absolute calibration of thermopiles.[1] For accurate intensity measurements it is necessary to make measurements in spectral regions free from discrete structure and preferably in regions where the photoionization cross sections are not varying too rapidly. Until recently the position and even the existence of discrete structure was unknown.[2-5]

The photoionization cross sections were measured from the ionization threshold of the gas down to about 280 Å. Whenever possible the power law $k = C \lambda^a$ was applied to extrapolate the values of the absorption coefficients k down to the soft x-ray region where experimental data again became available. The parameters C and a are constants within a given shell. Thus, in the case of argon, data is given from threshold at 786 Å down to .01 Å. Helium and neon are the only other two gases whose cross sections are known from threshold to .01 Å.

In the vacuum UV spectral region most of the theoretical calculations and experimental measurements on the total photoionization cross sections of the rare gases have been made in He and Ne. Experimental results in A, Kr, and Xe are scarce and with the exception of argon non-existant below 600 Å. From 44.6 to .01 Å results are again available.

Most of the experimental cross section measurements are not known to better than ± 10% and in general the data points are too few to provide a detailed contour of the absorption curve. This is particularly

important in the case of He. All of the theoretical cross section curves of He lie within the experimental errors of the existing data and it is impossible to say which theoretical approach is the most promising. Thus improved accuracy of the absolute value of the cross section is required as is the accuracy of the spectral shape of the curves.

In this present work the absorption cross sections of He, Ne, A, Kr, and Xe have been measured from the photoionization threshold down to 280 Å. The accuracy in the absolute value of the cross sections are estimated at ± 5% and from 2-3% in the relative values. These results are compared to existing theories.

Discrete structure is discussed due to excitation of inner shell electrons and their energy levels predicted where they as yet have not been observed. A table of critical absorption energies has been compiled from the literature since no such table exists. Finally, a discussion of the oscillator strengths for transitions to the photoionization continuum is given for each of the rare gases.

II. EXPERIMENTAL PROCEDURE

Absorption coefficients were measured by the double ion chamber technique.[1] Figure 1 shows the ion chamber in detail. A complete discussion of this ion chamber is given in reference 1. Briefly, however, the essentials are that the two collector plates must be identical in length, and the slits must be held at a positive potential to drive all ions formed in the vicinity of the slit over to plate i_1. A guard ring at the end of the ion chamber provided a uniform field at the end of the second plate. Thus, all ions formed were collected by their respective collector plates. The absorption coefficient $\underline{k}$ was then given by

$$k = 1/x \ \ell n(i_1/i_2),$$

where x is the length of one collector plate reduced to S.T.P., i.e., $x = L(p/760)(273/T)$ where L is the actual path length in cm, p is the pressure in mm, and T the temperature in degrees Kelvin.

Two major advantages of this technique are (a) that the ion currents i_1 and i_2 are measured simultaneously and thus there is no demand that the light source intensity remain constant and (b) since the gas itself is the detector of the incident radiation it is insensitive to scattered radiation of wavelengths longer than its ionization threshold. However, some precautions do have to be considered. The most important one is that there is a danger of collecting electrons as well as ions. This occurs when the incident radiation can eject a photoelectron of sufficient energy to overcome the retarding potential of the collector plates.

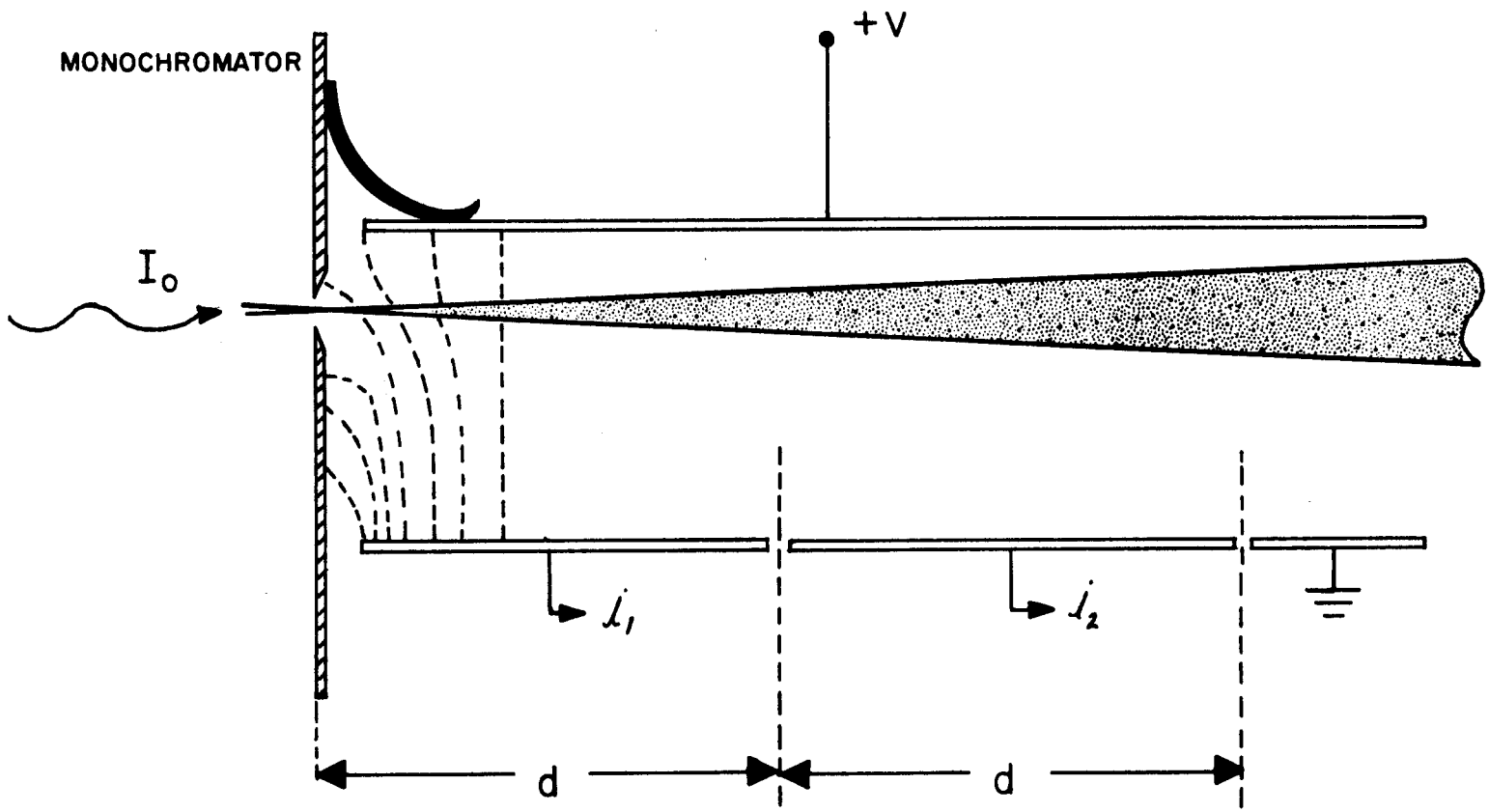

Figure 1. Absorption cell. The exit slit of the monochromator is held at the same potential as the repeller plate while a grounded guard plate at the end of the ion chamber provides a uniform field at the end of the second collector plate. Thus, all the ions formed under a given plate will be collected by that plate.

Sufficient voltage between the plates must be used to retard the most energetic electrons likely to be encountered. Secondary ionization by these energetic electrons also occurs and at first may appear to be a source of error. However, it can be shown[6] that the total ion current is proportional to $i_o e^{\alpha d}$, where i_o is the ion current when these secondary effects are absent, α, the first Townsend coefficient, is the number of ions created per cm/electron, and d is the separation of the ion plates. Thus, $e^{\alpha d}$ is a constant for any given gas, pressure, and wavelength. The ratio of the two currents i_1/i_2 should therefore remain constant and indeed this is found to be the case over quite a considerable range in voltage. Figure 2 shows a typical curve of ion current vs. voltage. The insert shows that i_1/i_2 varies little not only in the region where secondary ionization takes place but also in the region where electrons are being collected.

The vertical arrows a, b, and c represent, respectively, the ion chamber voltage necessary to start the retardation of the electrons, the voltage necessary to complete retardation, and the minimum voltage at which secondary ionization by electron collision is possible. In all runs, however, measurements were made within the plateau region of the ion current vs. voltage curve or as near to it as was possible.

The ion chamber was mounted on the exit arm of a Seya-monochromator, which was equipped with two interchangeable gratings. The gratings were both Bausch and Lomb replicas platinized to enhance their reflectivity at short wavelengths. The first order spectrum was increased by a factor

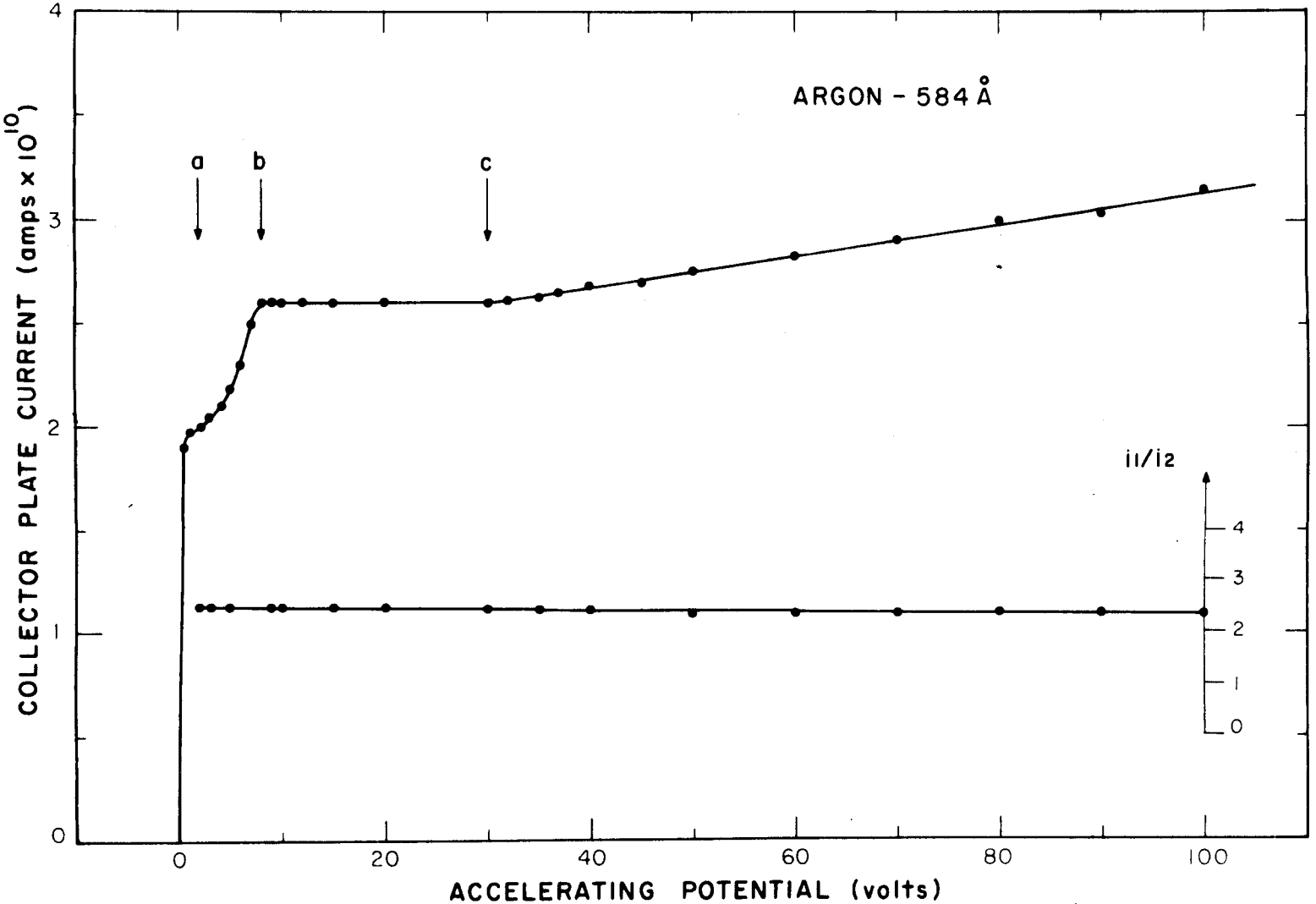

Figure 2. Typical ion current vs voltage curve. Argon was ionized by 584Å radiation thereby releasing electrons with approximately 5 eV energy. For the particular dimensions of the cell used the vertical arrows a, b, and c represent, respectively, the voltages at which retardation of the electrons start, finish, and at which the onset of secondary ionization occurs. The insert shows the variation of the ratio i_1/i_2 with voltage. There is a maximum variation of about 4% over the entire voltage range.

of five compared to the unplatinized condition. Wavelength separations of 2.6 Å and 1.3 Å were achieved with the 600 and 1200 line/mm gratings, respectively. The exit slit of the monochromator was 37 microns wide by 7 mm high. This small opening was used not only to provide maximum resolution but to reduce the flow rate of the gas within the ion chamber allowing accurate pressure measurements to be made. Figure 3 illustrates the complete experimental arrangement.

The light source consisted of a high voltage condensed spark discharge through a ceramic capillary. This produced a line spectrum characteristic of the gas used, which in this case was argon at approximately 0.1 Torr. The light source was separated from the monochromator by a two stage differential pumping unit. The first stage was evacuated by a 15 cu ft/min Welch mechanical pump while in the second stage a 4" diffusion pump was used. The main monochromator was also evacuated by a 4" diffusion pump. With this arrangement a negligible amount of the light source gas found its way into the ion chamber.

The all metal ion chamber had its own 2" diffusion pump which evacuated the chamber down to 1×10^{-5} Torr. After thorough pumping the 2" system was valved off. The ion chamber was then pumped on by the main monochromator pumps via the exit slit. A pressure of 1×10^{-4} Torr was then obtained. The gas under investigation was passed through a leak valve then a cold trap and finally into the rear of the ion chamber. The minimum pressure of the gas in all experiments was about 0.1 Torr. Thus, even if we assume that the dynamical flow of gas did not remove

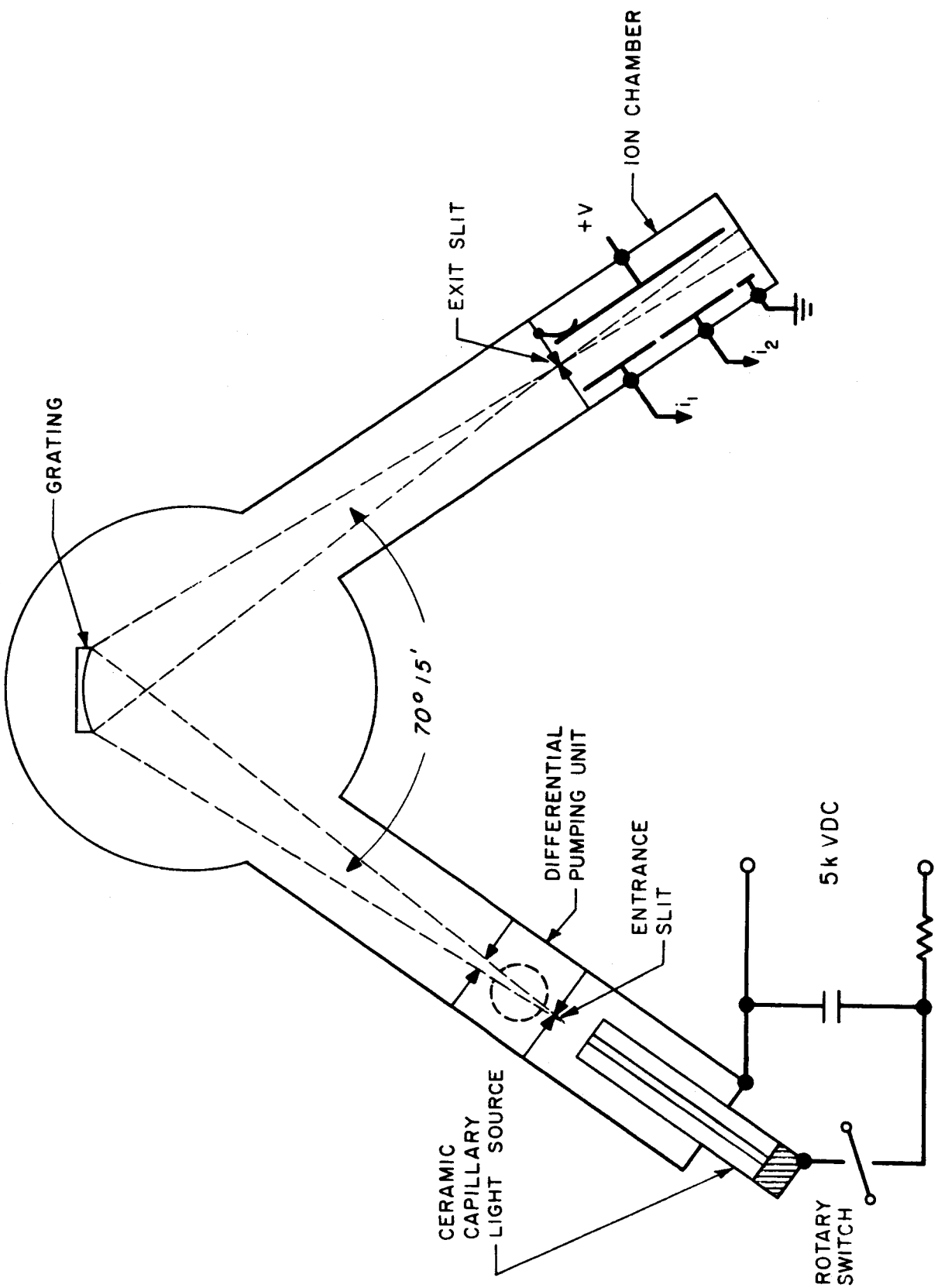

Figure 3. 1/2M Seya-Monochromator showing the experimental arrangement of light source, vacuum monochromator, and absorption cell.

some of the residual impurities we still have a purity ratio of 1000:1 at the minimum pressure.

Research grade gas from the Matheson Co. was used in the case of Ne, Kr, and Xe. Argon and helium were also obtained from the Matheson Co. with a quoted purity of 99.9%. Neon and helium were further purified by passing them through a liquid nitrogen cooled charcoal trap. The remaining gases were all passed through dry ice traps.

The two micro-microammeters used to measure i_1 and i_2 were calibrated to an accuracy of 1%. This was achieved by making a high impedance current source using a standard cell and Victoreen high meg-ohm resistors quoted to be accurate to within 1%. The micro-microammeters were used to drive two Leeds and Northrop recorders each of which had an accuracy of $\frac{1}{4}$% for full scale deflection.

Only radiation below the ionization threshold could contribute to the detectable scattered radiation. This scattered radiation was troublesome only below 400 Å since in this region the line spectrum was much less intense than at the longer wavelengths. Correction for the scattered radiation was performed as follows: A measure of the scattered light was made between 50-150 Å and was found to be constant. Since the monochromator produced no spectrum in this region the signal must be due entirely to scattered light. The constancy of the scattered light was assumed to hold up to 400 Å. This constant signal was then subtracted from the measured ion currents.

The ratio of the ion currents could be measured with considerable precision. The main source of error left was in measuring the absolute pressure of the gas. Although the gas flow was dynamic it was felt that no serious pressure gradients existed in the ion chamber. Measurements of $\underline{k}$ with different techniques yielded values within a few percent of each other. The major single error was in measuring the absolute gas pressure. This error was estimated to be 3% maximum. A McLeod gauge was used in all pressure measurements to eliminate accumulative errors due to the calibration of secondary pressure sensitive devices. However, a thermocouple pressure gauge was used to insure that the pressure of the gas remained constant during a run.

The absolute values of the absorption coefficients thus determined were estimated to have an error spread of ± 5% except where discrete structure existed and also for the weakest lines where the error was somewhat more. The error in the spectral shape of the absorption curves was dependent only on the error in the logarithm of i_1/i_2. Since the ratio of i_1/i_2 was always adjusted to be greater than 2 the error in i_1/i_2 was not magnified by taking the logarithm of the ratio. The error was estimated to be within ± 3%.

III. ABSORPTION CROSS SECTIONS

1. Helium

The photoionization cross sections of helium were first calculated by Vinti[7] and Wheeler[8] in 1933 using a hydrogenic approximation. In this approximation the inner electron is regarded as moving in a field of charge two while the outer electron, excited into the continuum, is assumed to be in a field of charge one. Later, calculations were performed by many investigators;[9-16] these calculations included the use of the more sophisticated Hartree and Hartree-Fock wavefunctions.

Available experimental cross sections[17-19] agreed with the theoretical values within their experimental errors, however, it was not possible to say which theoretical approach was the most satisfactory. The present work has endeavored to reduce the scatter in the experimental points and to improve the overall accuracy of the cross section measurements to enable a choice between the various calculations to be made.

All previous experimental cross section measurements have been made using the photographic plate as a detector of radiation and all depended on the incident radiation intensity remaining constant during the exposures taken with the absorption cell empty and then filled with helium. The difficulties and errors inherent in the above method were removed by using two ionization chambers in series as discussed in the last section. This is the first time this method has been applied to helium. The cross sections shown in Fig. 4 represent the average of four different

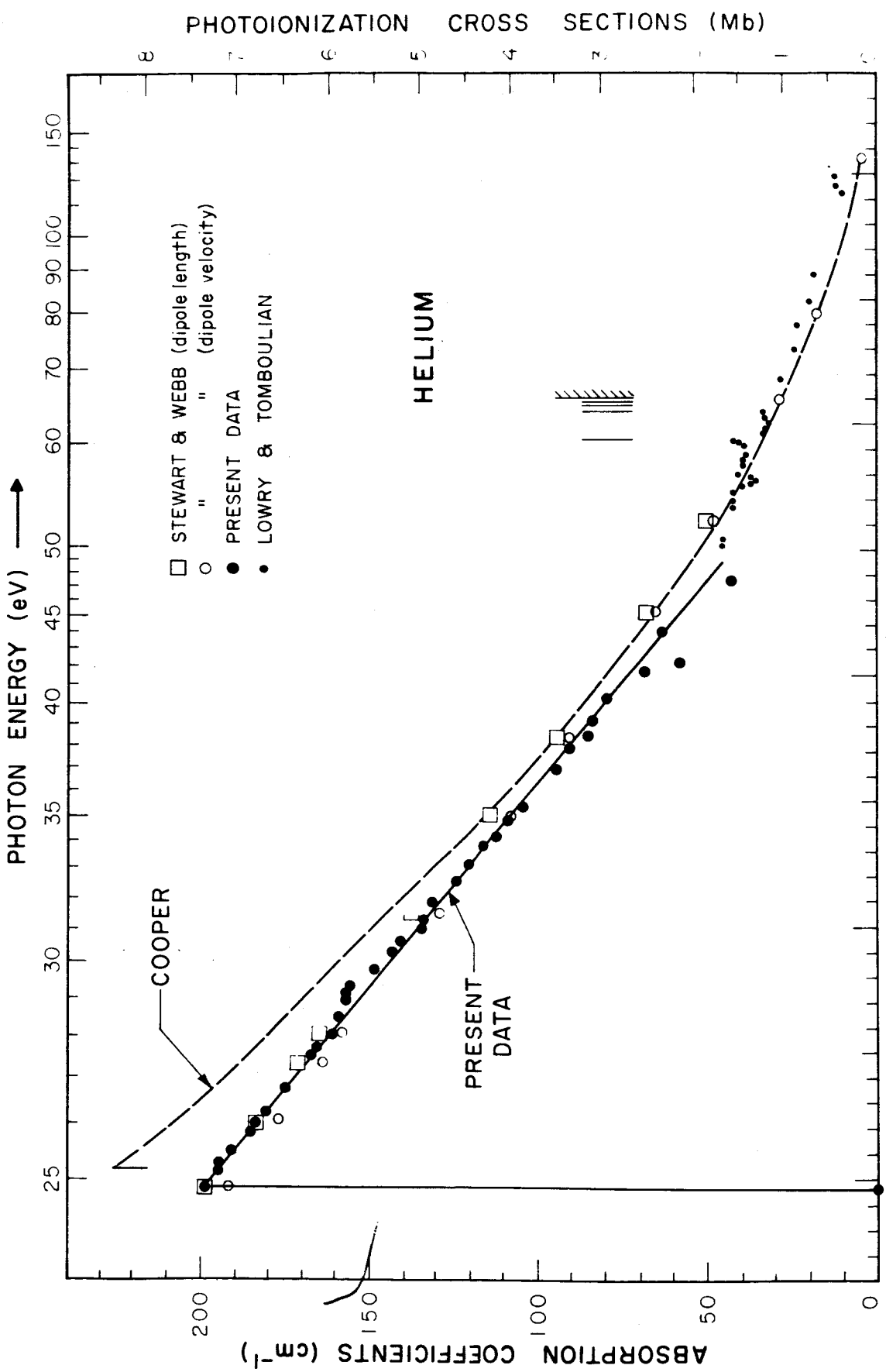

Figure 4. Photoionization cross sections of helium compared to theoretical values. The vertical lines indicate the position of discrete absorption lines due to double electron excitations.

determinations with the gas pressure varying from 0.5 to 1.0 Torr. The scatter of points lie within ± 2.5% of the average curve with the exception of the last few points at the shortest wavelengths where the spread is somewhat greater.

The vertical lines in Fig. 4 represent the positions of absorption lines discovered by Madden and Codling[2] using the continuum radiation from a 180 Mev synchrotron. They account for the series as being due to a double electron excitation process of the type $1s^2$-2s,np and $1s^2$-2p,ns. The first member of the series, appearing at approximately 260 Å, is common to the two series and represents the transition $1s^2\ {}^1S_o$-2s,2p $^1P^o$. Only one series was observed.

The data are compared with the theoretical calculations of Cooper,[16] who used a one electron model, and to that of Stewart and Webb[15] using the Hartree-Fock wavefunction. The experimental points of Lowry and Tomboulian[20] are included to extend the range of comparison down to 100 Å. The recent work of Stewart and Webb is felt to be the most sophisticated calculation of the helium cross sections available. They have computed the cross sections using the Coulomb, Hartree, and Hartree-Fock approximations and for each approximation they quote values using the dipole length, velocity, and acceleration formulations. We have selected the values obtained by the Hartree-Fock approximation as the ones which best fit our experimental data. It can be seen that the dipole length formulation is the best fit at the spectral head but at the shorter wavelenghts the velocity formulation appears superior. This is in agreement with the conclusion reached by Stewart and Webb.

It should be mentioned that the selected cross section values of Dalgarno and Stewart[12] are very close to those calculated by Stewart and Webb. The selected values were obtained from the data of Stewart and Wilkinson[14] for energies up to 1 rydberg and Haung's[10] acceleration values for energies greater than 1 rydberg; these values were then adjusted to provide good agreement with the various sum rules involving the oscillator strengths.

The experimental oscillator strength f for excitation into the continuum was obtained by using the relation

$$f = \frac{mc^2}{e^2 \pi n_o} \int k(\nu)\, d\nu \,, \qquad (1)$$

where k, the absorption coefficient, and ν the wavenumber are expressed in cm^{-1} and m, e, and c have their usual meaning. n_o is Loschmidt's number. The numerical value of $(mc^2)/(e^2 \pi n_o)$ is 4.19×10^{-8}.

The integral was evaluated graphically from the ionization threshold to .01 Å using the k-values tabulated in Tables I-III. A value of f = 1.54 was obtained. Since the contribution between .01 and 4.0 Å amounts to only .0001, the contribution below .01 is assumed to be negligible. The Thomas-Kuhn sum rule requires that the total oscillator strength be equal to the number of electrons in the atom, that is = 2 for helium. Thus, the contribution to the oscillator strength due to discrete structure must be = 0.46. Theoretical values for the discrete transitions have been calculated by several investigators.[7-13,21-23] A value of 0.45

TABLE I. Helium absorption coefficients from .01 to 44.6 Å

Shell	λ(Å)	Experimental[a] k(cm^{-1})	Semiempirical k(cm^{-1})
K	.010	---	$.0102 \times 10^{-3}$ ref. b
	.015	---	.0124 " "
	.020	---	.0141 " "
	.030	---	.0167 " "
	.04	---	.0187 " "
	.05	---	.0202 " "
	.10	---	.0250 " "
	.15	---	.0276 " "
	.20	---	.0293 " "
	.50	---	.0338 " "
	.80	---	.0386 " "
	1.00	$.045 \times 10^{-3}$	.0433 " "
	3.57	.463 "	---
	4.36	.819 "	---
	5.17	1.34 "	---
	6.97	3.20 "	---
	8.32	5.87 "	5.34×10^{-3} ref. c
	9.87	9.97 "	---
	13.37	22.43 "	21.36
	17.67	50.91 "	48.95 " "
	21.7	---	89.00 " "
	23.7	---	117.48 " "
	27.4	---	178.00 " "
	31.6	---	279.46 " "
	36.3	---	409.40 " "
	44.6	640.8 "	765.40 " "

[a] Determined from the mass absorption coefficients compiled by S.J.M. Allen in A. H. Compton and S. K. Allison, X-Rays in Theory and Experiment, (D. Van Nostrand Company, Inc., New York, 1935), p. 799.

[b] J. A. Victoreen, J. Appl. Phys. 20, 1141 (1949).

[c] B. L. Henke, J. Appl. Phys. 28, 98 (1957).

TABLE II. Helium absorption coefficients from 100-247 Å[a]

Shell	λ(Å)	k(cm^{-1})	λ(Å)	k(cm^{-1})	λ(Å)	k(cm^{-1})
K	100.90	12.9	144.82	19.6	198.03	31.9
	104.81	11.6	147.27	19.0	200.68	32.1
	107.00	9.8	151.51	19.0	202.32	32.9
	110.48	9.8	153.94	22.6	203.86	32.7
	115.82	9.6	156.18	22.1	207.24	41.9
	116.38	9.9	159.36	22.5	207.79	40.2
	117.85	11.0	160.10	21.9	209.28	38.1
	118.97	11.2	162.47	22.3	213.09	37.8
	122.25	12.2	164.60	23.5	214.25	38.3
	124.58	12.8	166.17	22.3	215.20	39.4
	125.23	14.9	168.08	23.8	216.02	38.3
	126.06	13.4	170.21	24.0	220.35	40.5
	128.26	13.4	171.09	24.4	221.65	36.5
	129.83	13.3	173.01	24.7	222.77	35.4
	131.80	13.9	177.75	25.6	223.78	36.5
	132.22	14.2	181.21	26.0	225.20	38.6
	132.84	14.2	182.40	28.4	227.53	42.1
	133.35	14.4	184.04	31.6	231.20	42.7
	135.52	15.1	185.74	30.2	233.52	42.1
	138.07	15.4	188.44	32.1	246.20	44.8
	139.02	16.0	192.82	29.2	247.60	44.8
	140.07	17.4	195.95	32.7		

[a] J. F. Lowry and D. H. Tomboulian, The K-Photoionization Cross Sections of Helium from 100 Å to 250 Å, Tech. Rep. No. 3, ARO(D) Project No. 2810P. The cross sections tabulated in this report have been converted to absorption coefficients by the relation $k(cm^{-1}) = 27\sigma(Mb)$.

TABLE III. Helium absorption coefficients from 262 Å to threshold.[a]

Shell	λ(Å)	k(cm^{-1})	λ(Å)	k(cm^{-1})
K	262.1	43	405.7	140
	283.1	60	410.6	143
	294.1	58	416.6	148
	297.9	69	423.3	156
	308.4	80	425.5	157
	317.7	84	429.7	157
	323.2	85	436.5	160
	329.3	91	442.8	163
	338.1	95	448.8	166
	352.2	103	452.0	167
	357.5	108	464.4	174
	364.0	113	473.6	180
	368.4	117	478.0	184
	375.7	120	482.0	185
	382.1	124	489.3	191
	390.6	132	494.3	195
	394.0	133	498.4	196
	397.1	133	503.0	198
	400.3	134	504.26	---

[a] Present data.

TABLE IV. Helium f-values for the transition 1^1S-n^1P as obtained from the relation $f = C/n^3$.

n	Dalgarno and Stewart[a]	Present data $f = C/n^3$
2	.270	.229
3	.0746	.0679
4	.0304	.0286
5	.01530	.0147
6	.00878	.00848
7		.00505
8		.00359
9		.00251
10		.00183

[a] A. Dalgarno and A. L. Stewart, Proc. Phys. Soc. 76, 49 (1960).

was obtained by both Dalgarno and Stewart,[12] and by Salpeter and Zaidi.[13] The calculations included the f-values for the doubly excited transitions as well as those for the resonance series. Since Dalgarno and Stewart quote f-values only for n = 2 to 6 the remainder of the sum for n = 7 to ∞ was obtained from their earlier paper.[11]

Discrete transitions for large n have f-values given, approximately, by $f = C/n^3$,[24] where n is the principal quantum number and C is given by twice the value of $df/d\epsilon$ evaluated at the series limit ($k = 217\ df/d\epsilon\ cm^{-1}$); ϵ being the kinetic energy of the released photoelectron measured in rydbergs. Using the present experimental data we find C = 1.83. Table IV compares the results of Dalgarno and Stewart with the values obtained from the above relation. As n increases we find the two results in good agreement.

2. Neon

As in helium, the photoionization cross sections of neon were treated theoretically many years before the first experimental results were available. The early results by Bates[25] in 1939 gave the value of the photoionization cross section of neon at its spectral head as $5.8 \times 10^{-18} cm^2$, in good agreement with later experimental results.[26,27] More recently Seaton[28] and Cooper[16] have published theoretical treatments. Seaton has calculated the cross section down to and including the L_1 edge, which involves absorption by the 2s electrons. Cooper does not compute the contribution of the 2s electrons and hence his curve does not show

the L_1 absorption discontinuity. The theoretical curves of Seaton and Cooper are reproduced in Fig. 5 along with the present experimental results.

Previous experimental work by Po Lee and Weissler[26] and also by Ditchburn[27] give cross sections which are from 15 to 20% lower than those presented here. Further, their curves rise more steeply from the spectral head and fall off more sharply near the L_1 edge. The recent work by Ederer and Tomboulian[29] provides the only other experimental data available. As in earlier experiments they used the photographic method of recording the incident radiation intensity with the exception, however, of using a Geiger counter at several selected wavelengths. Instead of filling the spectrograph with neon as was done by the previous investigators they used a small absorption cell with thin Zapon windows. The cell was located between the entrance slit and the grating. Thus, the present experimental techniques differ in many ways from all the previous methods. Briefly, the present method utilizes a windowless absorption cell located behind the exit slit. The incident and transmitted radiation is measured simultaneously by using the double ion chamber as a detector of the radiation. It is this last technique which is mainly responsible for reducing the scatter in the experimental points. As in the case of helium, the reagent grade neon was passed through a liquid nitrogen cooled activated charcoal trap for further purification before it entered the absorption chamber.

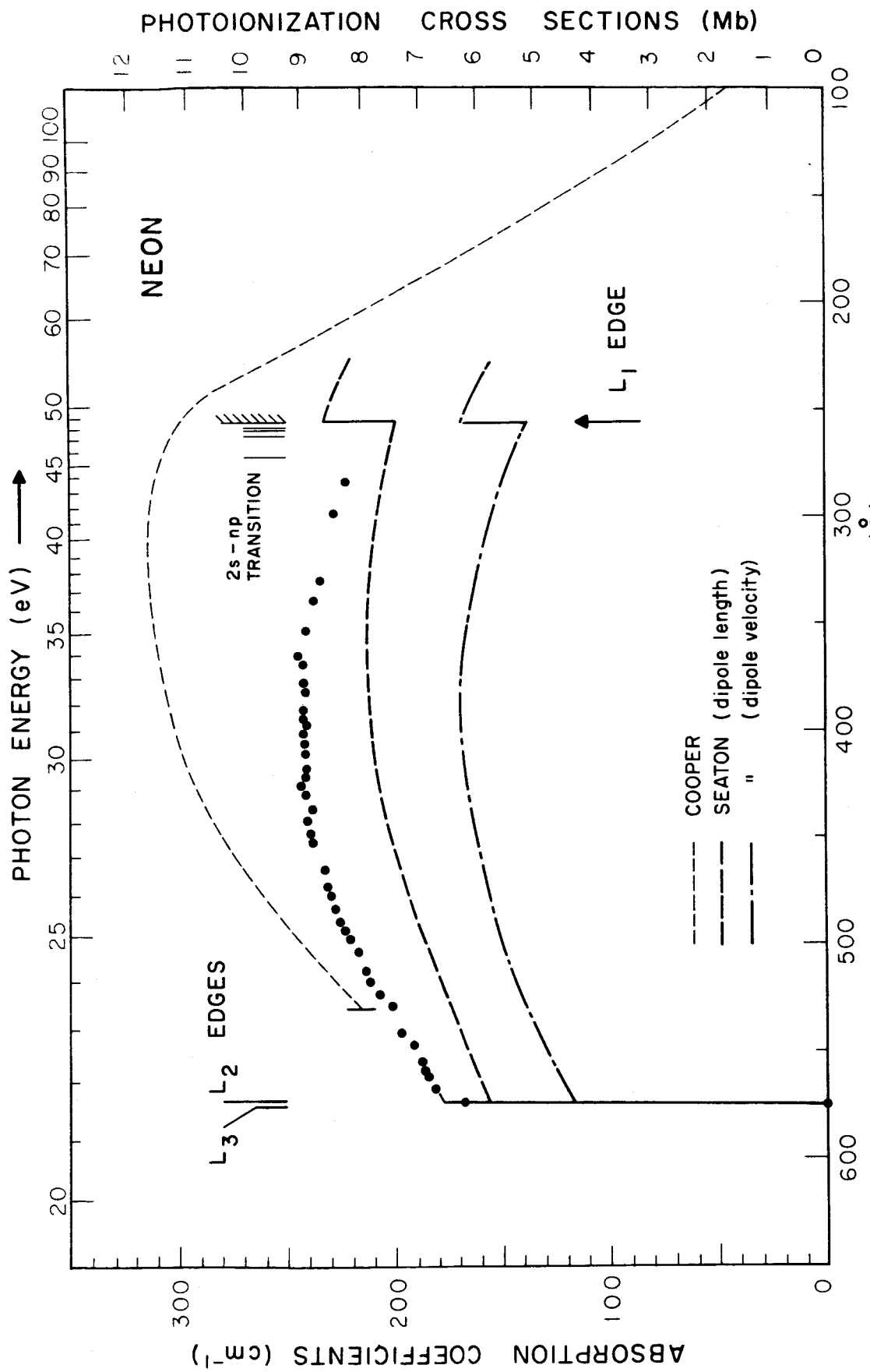

Figure 5. Photoionization cross sections of neon compared to theoretical values.

The experimental results are shown in Fig. 5 and are compared with the theoretical curves of Seaton and Cooper. Seaton's dipole length approximation is the closest fit to the experimental results, especially at the spectral head. Both approximations reproduce the spectral shape of the absorption curve. Cooper's one electron model, however, deviates somewhat more in its spectral shape. His curve agrees with the general experimental shape by increasing to a maximum and then decreasing, however, the position of the maximum is located at shorter wavelengths.

The vertical lines shown in Fig. 5 indicate the position of the absorption series due to the transition $2s^2 2p^6\ {}^1S_o - 2s2p^6 np\ {}^1P_1{}^o$ as observed by Madden and Codling.[2]

The oscillator strength for transitions into the continuum was measured graphically from threshold to .01 Å. An f-value of 10.03 was obtained. The data used to obtain the f-values are given in Tables V-VII. The contribution from the K-shell was 1.81. The variation of k with λ in the region between 100 Å and the K-edge (14.3 Å) can be expressed using the relation

$$k = 5.7 \times 10^{-4}\ \lambda^{2.6}$$

where k is in cm^{-1} and λ is in Å. This is essentially the same relation used by Ederer.[29] Using the sum rule, f for the continuum and discrete absorption lines must be equal to 10. Since the error limits are unknown for the data in Table V we cannot assign an experimental error to the value f = 10.03 and thus cannot predict the total discrete oscillator

TABLE V. Neon absorption coefficients from .01 to 44.6 Å.

Shell	λ(Å)	Experimental[a] k(cm^{-1})	Semiempirical k(cm^{-1})
K	.01	---	$.051 \times 10^{-3}$ ref. b
	.02	---	.071 " "
	.03	---	.084 " "
	.05	---	.102 " "
	.08	---	.121 " "
	.098	$.133 \times 10^{-3}$	---
	.100	---	.131 " "
	.130	.143 "	---
	.175	.166 "	---
	.200	.189 "	---
	.260	.243 "	---
	.417	.522 "	---
	.497	.837 "	---
	.631	1.62 "	---
	.710	2.25 "	---
	.880	4.09 "	---
	1.00	5.85 "	---
	1.235	11.16 "	---
	1.389	15.3 "	---
	1.54	21.6 "	---
	1.934	44.1 "	---
	2.500	90 "	---
	3.57	247 "	---
	4.36	430 "	---
	5.17	687 "	---
	6.97	1554 "	---
	8.32	2475 "	2487.000×10^{-3} ref. c
	9.87	3879 "	---
	13.37	7650 "	7416 " "
	14.298	---	---
L	17.6	---	971 " "
	21.7	---	1677 " "
	23.7	---	2141 " "
	27.4	---	3218 " "
	31.6	---	4725 " "
	36.3	---	6876 " "
	44.6	11790 "	11860 " "

[a] Determined from the mass absorption coefficients compiled by S.J.M. Allen in A.H. Compton and S.K. Allison, X-Rays in Theory and Experiment, (D.VanNostrand Co., Inc., N.Y., 1935), p. 799.

[b] J. A. Victoreen, J. Appl. Phys. 20, 1141 (1949).

[c] B. L. Henke, J. Appl. Phys. 28, 98 (1957).

TABLE VI. Neon absorption coefficients from 80 to 283 Å.

Shell	λ(Å)	k(cm^{-1})	λ(Å)	k(cm^{-1})
L	80.57	67.2	195.95	195.8
	83.50	68.0	202.32	203.3
	85.32	74.3	203.86	200.1
	90.40	81.3	207.24	206.3
	96.58	71.3	209.28	204.7
	99.60	77.8	214.25	209.0
	104.81	91.3	215.20	207.6
	110.48	100.4	218.50	207.0
	115.82	99.9	220.35	217.6
	117.85	102.3	227.52	220.9
	118.97	104.8	228.00	213.0
	129.83	118.8	231.20	221.7
	133.45	127.2	233.52	221.4
	135.52	129.1	238.47	222.2
	138.07	133.7	241.50	212.0
	150.01	152.6	243.02	220.0
	151.50	151.7	246.20	231.9
	159.36	160.9	247.60	230.9
	162.47	164.4	248.60	240.0
	164.60	164.2	251.50	225.0
	166.17	168.2	256.31	230.0
	168.08	170.1	260.45	236.0
	172.16	177.7	263.45	237.6
	173.01	183.1	266.95	230.0
	184.04	182.5	267.50	212.0
	185 ±5	187.0	277.30	206.6
	185.74	191.7	283.50	216.0
	192.82	191.2	282.32	215.7
	194.59	182.8		

[a] D. L. Ederer and D. H. Tomboulian, Tech. Rep. No. 10, Contract No. Nonr-401(37), (June 1963).

TABLE VII. Neon absorption coefficients from threshold to 200 Å.[a]

Shell	λ(Å)	k(cm^{-1})	λ(Å)	k(cm^{-1})
L	283.1	224	448.8	240
	297.9	228	452.0	239
	329.3	236	464.4	234
	338.1	238	473.6	231
	352.2	241	478.0	230
	364.0	245	482.0	228
	368.4	243	489.3	225
	375.7	243	494.3	223
	382.1	242	498.4	221
	390.6	242	503.0	218
	394.0	241	511.0	214
	397.1	241	516.1	212
	400.2	243	521.6	209
	405.7	243	528.7	202
	410.6	243	541.4	198
	416.6	242	546.9	193
	423.3	242	553.5	188
	425.5	243	558.0	186
	429.7	242	561.6	185
	436.5	239	567.5	182
	442.8	240	573.5	168
			574.93	---

[a] Present data.

strengths. Theoretical calculations have been made on the values of the discrete oscillator strengths by Cooper[16] and by Gold and Knox.[30] Gold and Knox obtained an f-value of 0.11 for the 736 Å line and .011 for the 742 Å line. From Cooper's calculations the 2p-nd and the 2p-ns transitions were estimated to contribute 0.3 to the discrete oscillator strengths. An experimental value f = .2 for the 736 Å line is quoted by Landolt and Börnstein.[31] Using this value and assuming the relation $f = C/n^3$ to hold for $n \geqslant 4$ we find a value f = 0.27. As defined previously, $C = 2\ df/d\epsilon$ where $k = 217\ df/d\epsilon$ and is measured at the spectral head. From all the above considerations if we estimate a total discrete oscillator strength to be 0.3 we then get a total f-value of 10.33 in good agreement with the sum rule.

In the case of neon, k-values in the photoionization continuum would need to be known to an accuracy better than 4% in order to determine the total discrete oscillator strength more accurately for comparison with theory.

3. Argon

Absorption cross section measurements in argon have been made by several investigators.[32-35] Their respective values disagree by as much as 10 to 50% Further, no published data exist which show the detailed spectral shape of the absorption curve from threshold to beyond 600 Å. With the exception of some concurrent work by Tomboulian and Ederer[36] and by Rustgi[37] no cross section data are available between 400 Å and the L-absorption edge at 50 Å.

The present experimental results are shown in Fig. 6. A preliminary report of these measurements has been published previously.[38] The absorption coefficients were measured from threshold to 280 Å. The vertical lines in Fig. 6 between the $^2P_{3/2}$ and $^2P_{1/2}$ levels simply indicate, schematically, the Beutler absorption lines which overlap the $^2P_{3/2}$ continuum.[39]

The theoretical[40] value of $\underline{k}$ at the spectral head is in excellent agreement with the experimental value of 840 cm^{-1}. In the calculations no distinction was made between the two edges; thus, we have reporduced the point on the $^2P_{1/2}$ edge for a clearer comparison.[41] The theoretical model of Cooper's[16] provides $\underline{k}$-values of the correct order of magnitude, however, the spectral shape of the absorption curve shows an immediate decrease in the absorption coefficients to wavelengths shorter than the $^2P_{1/2}$ edge in contradiction to the present experimental data. Recent experimental work by other groups[37,42] over the same spectral region confirm our spectral shape, and their $\underline{k}$-values agree within a few percent of those reported here.

Discrete absorption structure due to excitation of the inner s-electrons can be seen starting at 466 Å and ending with the removal of the s-electron at 424 Å. The unusual decrease in absorption for excitation of the 3s electrons is due to configuration interaction between the discrete states and the underlying continuum.[43] An excellent photograph of this series is given by Madden and Codling,[2] while a discussion of the Rydberg series is given in reference 4.

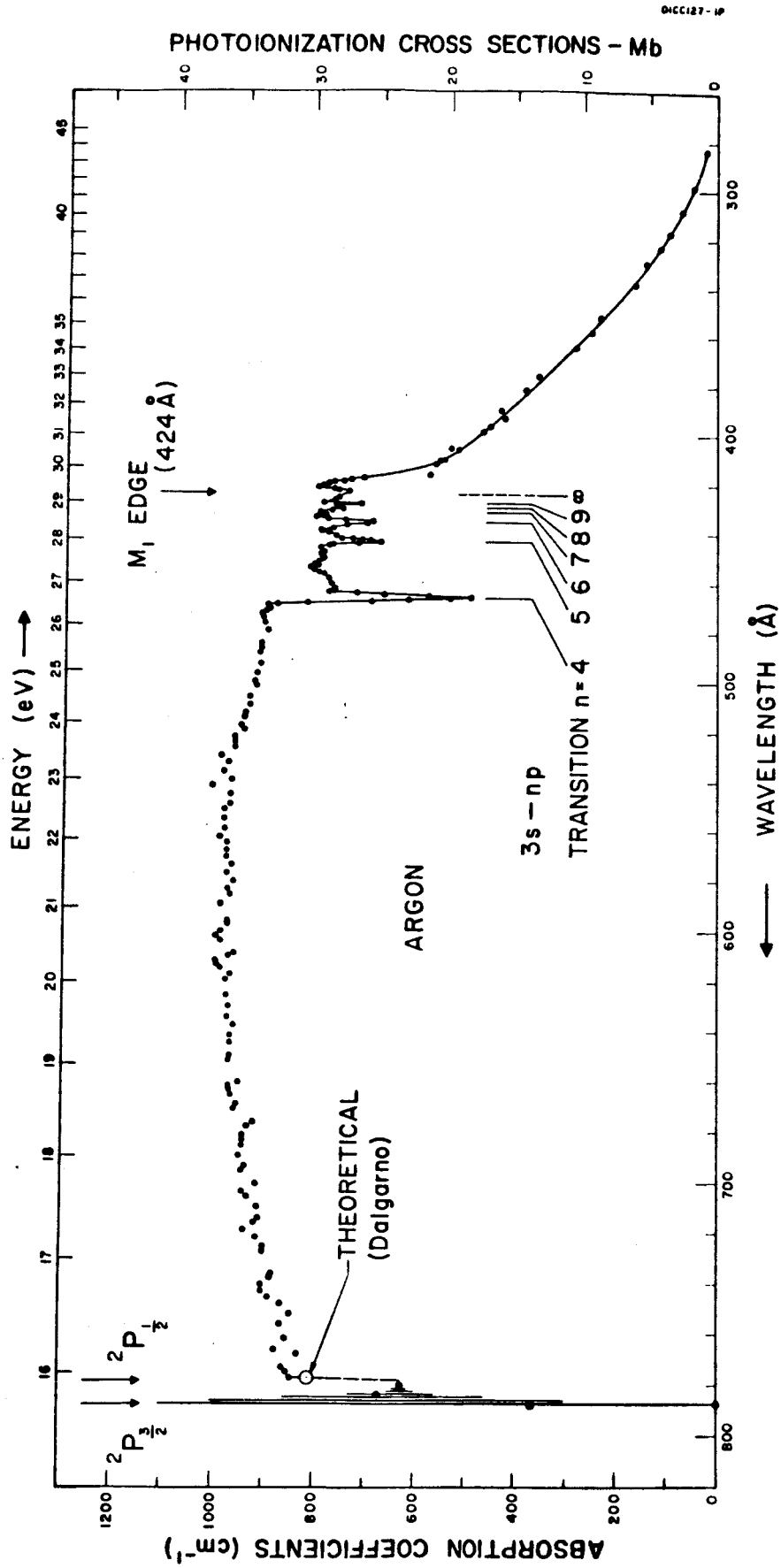

Figure 6. Photoionization cross sections of argon. The vertical lines between the $^2P_{3/2,1/2}$ edges indicate schematically the Beutler autoionization lines.

Relative photoionization cross sections σ_i in argon were first measured by Weissler et al.,[44] using a mass spectrometer. From the definition of the photoionization yield, γ, it can be shown[45] that

$$\sigma_i \cong C(i/I),$$

where C is a constant for any given pressure and path length, i is the ion current, and I is the relative photon intensity. The approximation is very good provided $kx \ll 1$, where k is the absorption coefficient and x is the path length reduced to S.T.P. In measuring I it is necessary to have a detector with a flat response as a function of wavelength; normally sodium salicylate is used.

Recently, Schönheit[46] published a more detailed curve of the relative cross sections using a mass spectrometer and a line emission light source similar to that used above. His very low relative cross section value at 466 Å is undoubtedly due to the 3s-np excitation.

Comes and Lessmann,[47] also using a mass spectrometer, studied the relative cross sections down to 685 Å. They observed considerable apparent structure to the short wavelength side of the $^2P_{1/2}$ edge. This structure is not apparent in the present work nor in any work using the conventional absorption techniques. Although some scatter of points is observed above the $^2P_{1/2}$ edge in Fig. 6 no significance is placed on them at this time. It may be possible that weak excitations in a strong ionization continuum are more easily observed at the low pressures used in the relative cross section measurements.

In the present work the absorption coefficients decrease from the M_1 edge according to the relation,

$$\underline{k} = 2.35 \times 10^{32} \lambda^{5.5}, \qquad (1)$$

where $\underline{k}$ is measured in cm^{-1} and λ in cm.

Thus, we are able to estimate the values of the absorption coefficients down to the L-edge at 50 Å. There is no theoretical basis for Eq. (1) and one must be careful in extrapolating such a relation over an extended wavelength region. However, in all probability, coefficients can be estimated within an order of magnitude. Preliminary data by Ederer and Tomboulian[36] give $k = 36.5\ cm^{-1}$ at 182.2 Å, whereas Eq. (1) yields only $6.4\ cm^{-1}$.

Table IX lists the experimentally determined absorption coefficients from threshold down to 280 Å. In Table VIII absorption coefficients are listed from 44 - .01 Å as obtained from the data compiled by Allen[48] and the semiempirical values determined by Henke[49] and Victoreen.[50]

Using the coefficients tabulated in Tables VIII and IX, and applying Eq. (1) to the interval 50-300 Å, one obtains the oscillator strength for transitions into the continuum, using the relation

$$f = 4.19 \times 10^{-8} \int k(\nu)\, d\nu.$$

The integral was carried out graphically for the data in the Tables. The K-shell contributes 1.77 down to .01 Å, the L-shell gives 7.51, and the M-shell a value of 5.65, excluding the region between the $^2P_{1/2,3/2}$

TABLE VII[1]. Argon absorption coefficients from .01 to 44.6 Å.

Shell	λ(Å)	Experimental[a] k(cm^{-1})	Semiempirical k(cm^{-1})
K	.01	---	$.092 \times 10^{-3}$ ref. b
	.02	---	.128 " "
	.03	---	.153 " "
	.05	---	.190 " "
	.08	---	.247 " "
	.098	$.328 \times 10^{-3}$	---
	.100	---	.293 " "
	.130	.437 "	---
	.175	.714 "	---
	.200	.794 "	---
	.260	1.510 "	---
	.417	5.260 "	---
	.497	8.93 "	---
	.631	17.45 "	---
	.710	23.2 "	---
	.880	42.9 "	---
	1.000	62.5 "	---
	1.235	111.0 "	---
	1.389	153.0 "	---
	1.540	211.0 "	---
	1.934	420.0 "	---
	2.500	846.0 "	---
	3.570	2160.0 "	---
	3.870	2610.0 "	---
L	3.870	263.0 "	---
	4.360	360.0 "	---
	5.170	578.0 "	---
	6.970	1335.0 "	---
	8.320	2070.0 "	2076.000×10^{-3} ref. c
	9.870	3320.0 "	---
	11.90	5530.0 "	---
	13.3	---	6760 " "
	17.6	---	12680 " "
	21.7	---	19720 " "
	23.7	---	24150 " "
	27.4	---	33700 " "
	31.6	---	45800 " "
	36.3	---	61950 " "
	44.6	81600.0 "	---
	50.6	---	---

[a] Determined from the mass absorption coefficients compiled by S.J.M. Allen in A.H. Compton and S.K. Allison, X-Rays in Theory and Experiment, (D VanNostrand Co., Inc., N. Y., 1935), p. 799.

[b] J. A. Victoreen, J. Appl. Phys. 20, 1141 (1949).

[c] B. L. Henke, J. Appl. Phys. 28, 98 (1957).

TABLE IX. Argon absorption coefficients from threshold to 280 Å.[a]

λ(Å)	k(cm^{-1})	λ(Å)	k(cm^{-1})	λ(Å)	k(cm^{-1})	λ(Å)	k(cm^{-1})
282.8	23	436.9	768	471.3	900	618.8	981
297.8	47	437.5	770	474.0	912	625.2	978
308.0	72	438.1	796	475.7	909	629.8	973
317.3	98	438.8	794	479.4	900	634.0	978
323.0	115	439.4	780	484.2	912	637.0	964
329.0	143	440.0	768	486.8	912	641.0	971
337.6	167	440.7	763	487.9	915	644.1	971
351.0	233	441.3	757	492.5	915	649.0	971
357.6	253	441.9	731	496.5	924	651.0	973
363.8	285	442.1	712	499.4	926	660.0	952
375.2	360	442.6	695	501.3	924	662.7	971
381.6	382	443.2	673	505.8	936	664.8	968
389.9	434	443.8	720	509.3	936	668.3	956
393.3	426	444.2	773	512.1	945	670.2	960
396.5	454	444.5	778	514.3	945	675.2	924
399.3	466	445.1	796	517.5	952	677.1	936
405.2	535	445.7	796	519.5	945	680.5	945
405.7	520	446.4	796	521.9	964	683.0	945
410.0	558	447.9	788	524.2	964	684.8	945
411.5	562	449.8	787	526.7	964	688.4	950
416.9	709	450.2	790	529.3	991	692.8	940
417.6	734	450.8	808	532.0	978	694.9	945
418.2	750	451.4	800	536.0	985	700.0	915
418.8	769	452.1	808	539.3	971	703.0	945
419.4	781	452.7	798	541.8	999	705.4	934
420.0	790	453.3	817	544.9	973	709.2	915
420.7	800	453.9	810	549.3	973	713.7	912
421.3	767	454.5	810	551.4	985	715.5	920
421.8	760	455.2	800	555.1	985	718.4	940
422.4	738	455.8	790	558.8	985	721.0	915
425.2	762	457.0	783	562.1	995	724.8	900
425.8	767	457.6	780	564.6	981	727.2	900
426.4	767	459.8	778	567.9	981	735.6	883
427.0	790	462.2	768	570.4	981	737.0	887
427.7	712	462.5	768	573.7	971	739.9	906
428.3	764	463.1	760	577.0	978	742.4	905
428.9	760	463.7	723	580.0	964	744.6	890
429.5	752	464.4	669	583.0	978	747.5	865
430.1	773	465.0	579	585.5	973	751.1	845
430.9	798	465.6	492	588.9	990	755.1	866
431.5	789	466.3	536	594.1	978	760.6	856
432.2	787	466.6	619	596.7	978	765.3	876
432.9	804	466.9	695	599.5	991	767.3	830
433.7	782	467.6	822	603.4	991	772.4	860
434.2	747	468.2	882	608.5	964	774.6	852
434.5	692	468.7	900	610.0	973	776.8	845
435.0	703	468.8	897	613.0	998	779.7	627
436.0	742	469.5	900	614.8	991	783.2	671
436.5	766	470.1	897	616.7	973	787.6	364
436.7	770	470.8	900				

[a] Present data.

edges. If we consider the contribution to the oscillator strengths for discrete transitions in the K and L-shells then the above f-numbers approach 2 and 8, respectively. To find the total oscillator strength for the M-shell we must include the contribution from the resonance lines, the Beutler lines, and the continuum between the $^2P_{1/2,3/2}$ edges. The resonance f-values have been computed by Knox[51] yielding 0.2 (1048 Å) and .05 (1067 Å). An estimate of the remaining members of the series $3p^5ns'$ up to the $^2P_{3/2}$ threshold is given by

$$f_n = \sum_{n=5}^{10} C/n^3,$$

where C = 7.84. This gives f ≅ 0.355 for the resonance lines. Metzger et al.,[34] quote a total of .038 for the Beutler lines and the underlyind $^2P_{3/2}$ continuum. Thus, the total oscillator strength for the M-shell is 6.04. Since the Thomas-Kuhn sum rule requires f = 18 for argon and since the individual contributions from the K and L-shells are approximately 2 and 8, respectively, it might be suggested that the sum rule applies to each shell. This would then require that the M-shell contribute f = 8 in contrast to the estimated value of 6.04. Thus, either k does not decrease so rapidly as indicated by Eq. (1) or, possibly, that the absorption coefficients increase to some maximum value as indicated theoretically by Cooper.[16] In fact such an analysis of the experimental f-number as given above strongly favours Cooper's prediction that the absorption coefficients should start to increase below 300 Å. To clear up this point experimental absorption coefficients are necessary between 50 and 300 Å.

4. Krypton

The only theoretical treatment of krypton is that by Cooper.[16] As in argon, however, the theoretical absorption curve shows an immediate decrease from the $^2P_{1/2}$ spectral head, the decrease being concave down to the shortest wavelengths.

The experimental results, illustrated in Fig. 7, show an initial increase in the cross sections from the $^2P_{1/2}$ threshold coming to a maximum about 760 Å then decreasing to the N_1 edge. Prior to the N_1 edge discrete absorption dips are observed similar to those in argon. Their precise positions are indicated by the vertical lines as obtained with a flash tube continuum light source.[5] Similar absorption lines have been reported by Madden and Codling.[3] The N_1 edge is the x-ray terminology for the ionization potential of the 4s-electrons and is normally characterized by an abrupt increase in the absorption coefficient. However, in the case of the rare gases these abrupt changes either do not exist or are extremely small for the outer shells. As can be seen in Fig. 7 the absorption coefficients decrease smoothly before and after the N_1 edge. The recent Kr spectrum taken by Codling and Madden[52] in the vicinity of 130 Å also shows a smooth absorption curve on either side of the $M_{4,5}$ edge (that is, the ionization limit of the 3d-electrons).

Below the N_1 edge and between 350-185 Å the absorption curve can be fitted to the relation

$$k(cm^{-1}) = 1.4 \times 10^{-8} \lambda^4 (Å). \quad (1)$$

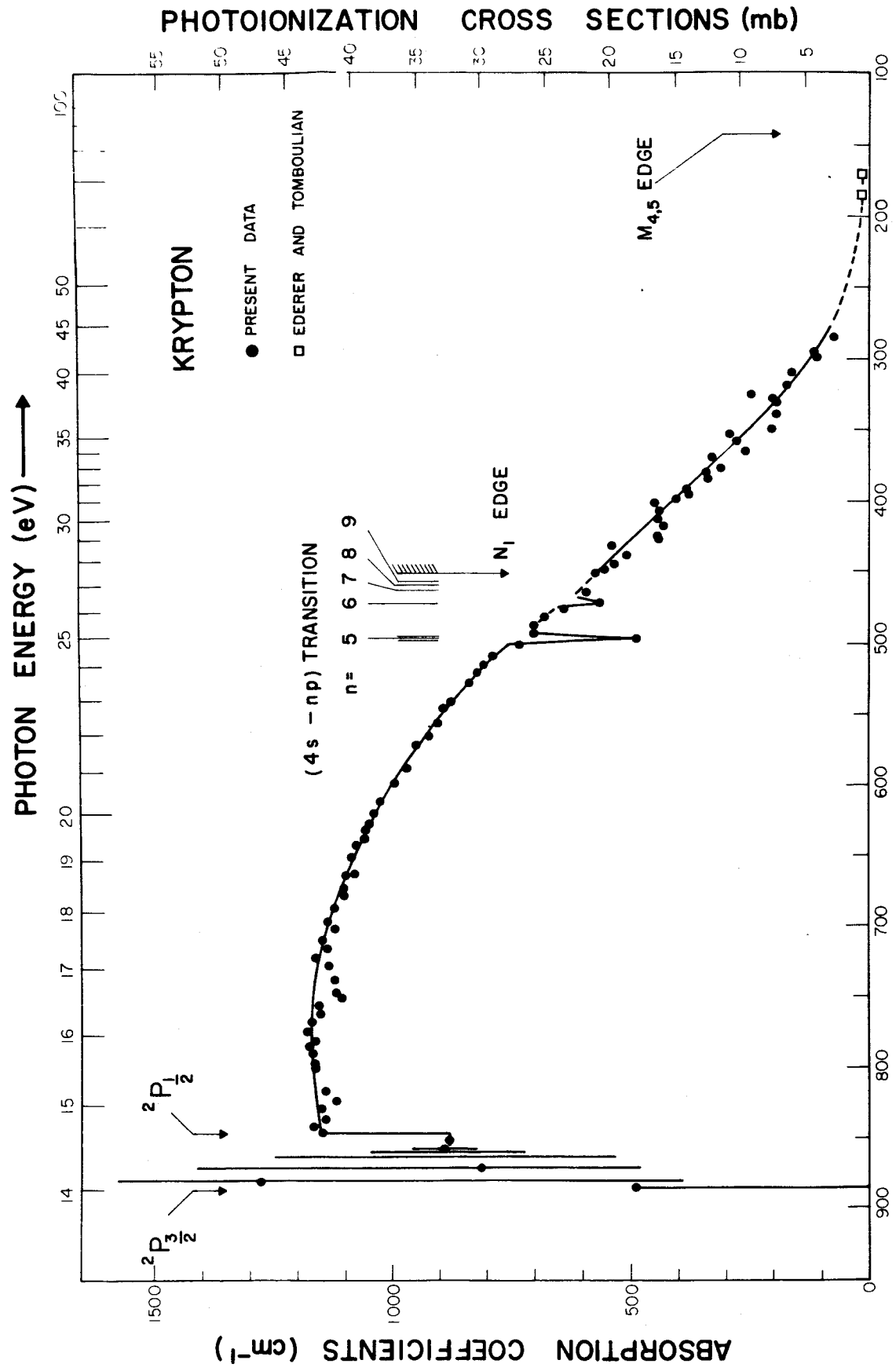

Figure 7. Photoionization cross sections of krypton. The vertical lines between the $^2P_{3/2,1/2}$ edges indicate schematically the Beutler autoionization lines.

This fits smoothly to the data points at 185 Å by Ederer and Tomboulian.[36]

The k-value at the spectral head ($^2P_{1/2}$) is found to be 1140 cm^{-1} ± 5% in excellent agreement with Pery-Thorne and Garton[53] who quote a value of 1120 cm^{-1} ± 18%. Other investigators [34,42,54,55] do not quote a value, however, from their curves they are in approximate agreement, with the exception of Huffman et al.[54] Their results are all about 15% higher than these presented here and may be due to their method of correcting for the pressure in a dynamic gas flow absorption cell. We have made no corrections since with our particular absorption cell the gas pressure appears to be uniform and stable.

Measuring the f-value from the $^2P_{1/2}$ threshold down to 284 Å we get f = 5.65. Extrapolating from 284 Å to the M_5 edge (132 Å) using Eq. (1) an f-value of 0.04 is obtained. The continuum and Beutler lines between the $^2P_{1/2,3/2}$ edges contributes 0.216 according to Metzger et al.[34] or 0.287 according to Huffman et al.[54] Taking the mean of the two values f = 0.252. The theoretical value[16] of the discrete transitions prior to the $^2P_{3/2}$ threshold are estimated to be approximately 0.5. This gives a total oscillator strength of 6.8 for the 4(sp) electrons down to the M_5 edge.

Table X presents the absorption coefficients in the K-shell from .01 to .8 Å and one point in the M-shell at 44.6 Å. The contribution to the continuum f-number due to the K-shell is measured to be 1.63 from the K-edge down to .01 Å. Table XI tabulates the coefficients from threshold to 284 Å.

TABLE X. Krypton absorption coefficients from .01 - .8 and at 44.6 Å

Shell	λ(Å)	Experimental[a] $k(cm^{-1})$	Emperical[b] $k(cm^{-1})$
K	.010	---	$.183 \times 10^{-3}$
	.012	---	.201 "
	.015	---	.227 "
	.020	---	.263 "
	.025	---	.298 "
	.030	---	.334 "
	.040	---	.414 "
	.050	---	.514 "
	.060	---	.649 "
	.080	---	1.037 "
	.098	2.08×10^{-3}	---
	.100	---	1.64 "
	.120	---	2.50 "
	.150	---	4.40 "
	.200	10.8 "	9.56 "
	.260	21 "	---
	.417	77 "	---
	.497	129 "	---
	.631	238 "	---
	.710	338 "	---
	.800	408 "	---
	.866	---	---
L	---	---	---
M	44.6	118000. "	---

[a] Determined from the mass absorption coefficients compiled by S.J.M. Allen in A. H. Compton and S. K. Allison, X-Rays in Theory and Experiment, (D. Van Nostrand Company, Inc., New York, 1935), p. 799.

[b] J. A. Victoreen, J. Appl. Phys. 20, 1141 (1949).

TABLE XI. Krypton absorption coefficients from threshold to 280 Å.[a]

λ(Å)	k(cm^{-1})	λ(Å)	k(cm^{-1})	λ(Å)	k(cm^{-1})	λ(Å)	k(cm^{-1})
283.7	73	416.6	428	564.6	923	736.8	1118
294.7	112	423.3	439	570.6	948	745.1	1116
298.5	106	425.5	435	586.0	972	748.1	1107
309.0	160	429.7	532	596.6	993	755.1	1154
318.2	169	436.5	498	609.8	1028	760.4	1151
323.7	244	442.8	527	618.9	1041	766.1	1169
327.0	202	447.3	549	625.6	1049	772.7	1180
329.8	193	450.6	570	630.2	1053	779.4	1157
338.5	193	462.8	591	636.6	1057	783.1	1176
349.5	201	471.4	562	640.8	1077	789.1	1164
352.6	291	474.4	634	644.6	1070	795.6	1162
358.0	278	479.4	675	649.7	1086	800.8	1161
364.4	256	487.2	695	660.6	1078	814.6	1091
368.7	325	492.2	699	663.6	1096	821.5	1116
376.0	305	496.3	483	671.1	1104	827.4	1153
380.0	340	500.8	727	675.6	1037	834.8	1140
382.4	333	508.8	785	685.0	1121	840.1	1167
390.7	376	514.6	303	694.6	1136	844.6	1147
394.0	374	519.6	815	700.6	1122	850.4	878
397.2	400	526.7	835	709.1	1146	857.6	891
400.3	449	539.6	877	714.1	1136	870.3	812
405.7	435	545.4	888	721.2	1163	878.6	1276
410.6	438	555.1	904	725.6	1132	883.6	488

[a] Present data.

5. Xenon

Until recently,[34,35] no data on the photoionization cross sections of xenon existed and at present there are no published data to wavelengths shorter than 600 Å. Further, no theoretical treatment of the xenon cross sections is available. However, some current experimental work is in progress below 600 Å.[36,55]

Figure 8 shows our experimental results. The data between 1020 Å and 850 Å were taken with a hydrogen DC glow discharge lamp. Since the hydrogen spectrum becomes too weak below 850 Å we are not troubled with second order lines within this range. This enables us to obtain an accurate value of the absorption cross section at the $^2P_{1/2}$ threshold, namely, 63 x 10^{-18} cm^{-2} (1700 cm^{-1}).

The Beutler lines are so broad that they can be resolved rather well using the many lined hydrogen spectrum. Since these lines have been studied rather extensively by Huffman *et al.*,[35] and by Metzger and Cook[34] no effort was made to improve the detail of the lines, rather, this work concentrates on the absolute cross sections and spectral shape of the ionization continuum below the $^2P_{1/2}$ edge. Below 850 Å the high voltage spark discharge light source was used. Between 700 and 850 Å we are still troubled to some extent by second order lines and care must be taken. The scatter in this region is probably due to these unwanted lines. Since the cross sections for the short wavelengths are so much lower than for the long wavelengths we are justified in drawing a curve through the higher valued data points in the

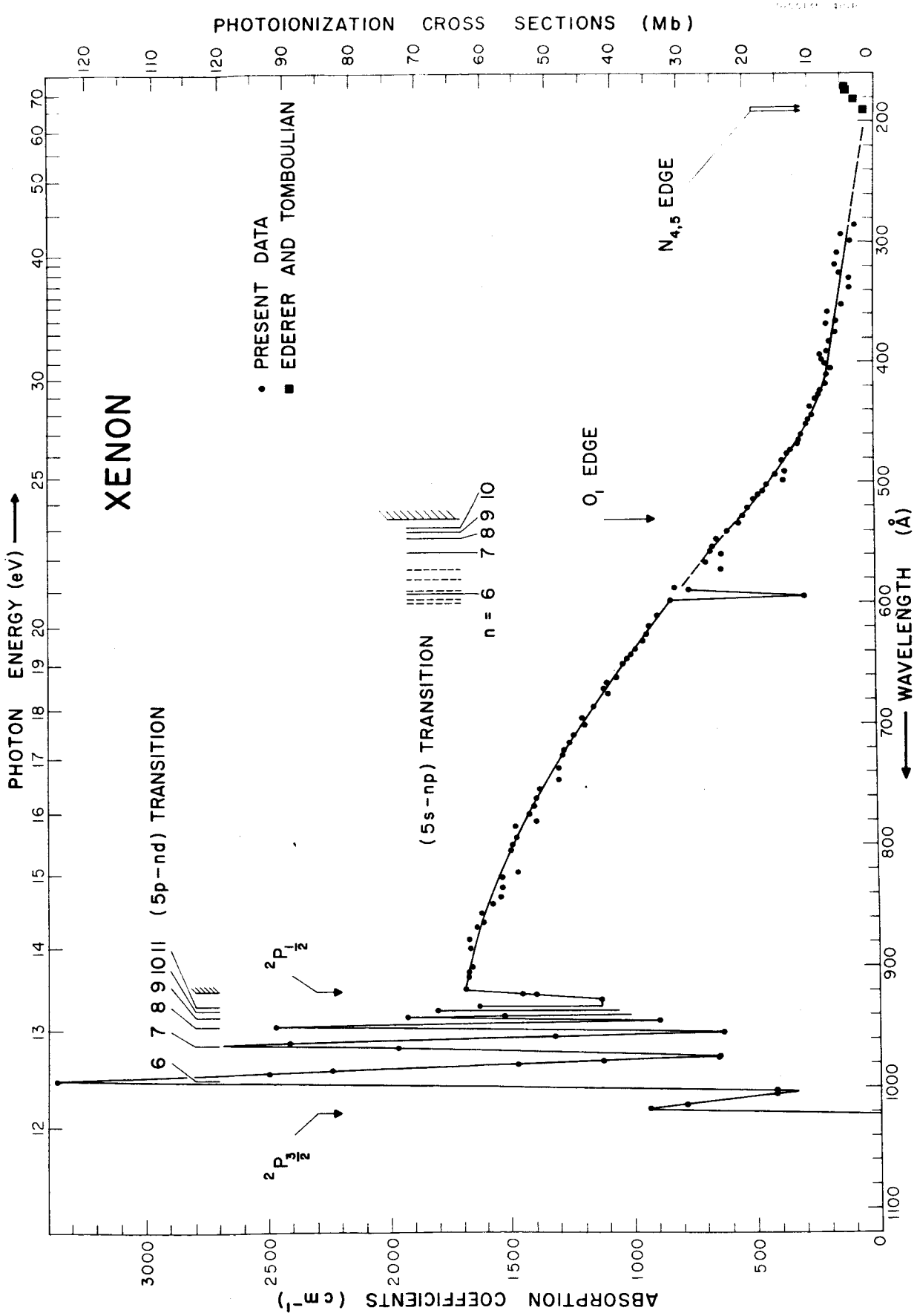

Figure 8. Photoionization cross sections of xenon. The data of Ederer and Tomboulian increase from the $N_{4,5}$ edge to a maximum of 30 Mb at 130Å.

region 700-850 Å.

The vertical lines in Fig. 8 show the position of the (5s-np) transition absorption lines as obtained using a flash tube continuum light source on a 2M normal incidence spectrograph.[5] The dashed lines also represent absorption lines which are as yet unclassified. The (5s-np) absorption series are all of the "window" type. That is they show a large decrease in absorption relative to the ionization continuum background. As in krypton no discontinuity at the O_1 edge was observed. The cross sections continue to decrease toward shorter wavelengths. Extrapolating this decrease from 280 Å we join smoothly onto the data of Tomboulian and Ederer[36] at the $N_{4,5}$ edge. Their data begins to increase at this point coming to a maximum of 30 Mb at approximately 125 Å, then decreases to 2 Mb at 80 Å.

From the onset of excitation of the inner shell electrons at 600 Å many discrete absorption lines exist down to the $N_{4,5}$ edge, due probably to double electron excitations. A recent spectrum by Codling and Madden[52] in the vicinity of 200 Å clearly shows the absorption series due to excitation of the 4d-electrons. Two series are observed terminating at the N_4 and N_5 edges, respectively. Again, no abrupt change in absorption is seen on passing over those critical edges. Their assigned limits to the two series at 178.33 Å and 183.55 Å provide the first experimental values of the critical absorption energies for the N_4 and N_5 edges of Xenon, respectively. These values compare favorably with the calculated ones of 183 Å and 191 Å.[56]

The assignment of these transitions as (4d-np) type transitions can be verified on the basis of the discussions given in Section IV-2. Briefly, this assigns a binding energy to electrons in the np shells (Table XVI). Adding these binding energies to the observed term values leads to consistent series limits within approximately ± 200 cm^{-1} of each other. On the other hand if the binding energies of the nf-electrons are added to the observed terms the resulting series limits lie within ± 6000 cm^{-1}. Since the f orbits are less penetrating the spread in the series limits should be much less than for p orbits. That this is not the case verifies the identification of the transition as (4d-np). It is of interest to note that given the series limit the wavelengths of the (4d-np) transitions can be readily calculated by the method described in Section IV. Using the 183.55 Å series limit quoted by Codling and Madden this technique predicts absorption lines at 190.63, 186.86, and 185.49 Å for n = 6, 7, and 8, respectively. These are to be compared with the values observed by Codling and Madden at 190.41, 186.81 and 185.47 Å.

The oscillator strength for transitions into the ionization continuum has been measured graphically from the $^2P_{1/2}$ edge down to 183.55 Å (N_5 edge). A value of f = 5.58 was obtained. The contribution from the continuum and Beutler lines between the $^2P_{3/2}$ and $^2P_{1/2}$ edges amounts to 0.43.[34] Recent experimental measurements[57] have estimated the discrete f-number for transitions into the $5p^5 6s$ configuration to be 0.61. This would then provide an approximate value of 6.62 for the contribution of the 5(sp) electrons down to the N_5 edge.

From Table XII the oscillator strength for the K-shell continuum is found to be 1.57 down to .01 Å. Table XIII gives f = 10.94 for the region between the N_5 and N_3 edges. That is, where the ten 4d electrons are absorbing. Table XIV lists the absorption coefficients for the present work.

TABLE XII. Xenon absorption coefficients from .01-.3 Å and at 44.6 Å.

Shell	λ(Å)	Experimental[a] $k(cm^{-1})$	Empirical[b] $k(cm^{-1})$
K	.010	---	$.287 \times 10^{-3}$
	.012	---	.318 "
	.015	---	.366 "
	.020	---	.444 "
	.025	---	.536 "
	.030	---	.646 "
	.040	---	0.946 "
	.050	---	1.39 "
	.060	---	2.02 "
	.080	---	3.94 "
	.098	8.2×10^{-3}	---
	.100	---	6.96 "
	.120	---	11.30 "
	.150	---	20.65 "
	.175	31.3 "	---
	.200	---	44.90 "
	.250	---	81.40 "
	.300	---	129.50 "
	.359	---	---
L	---	---	---
M	---	---	---
N	44.6	39500 "	---

[a] Determined from the mass absorption coefficients compiled by S.J.M. Allen in A. H. Compton and S. K. Allison, X-Rays in Theory and Experiment, (D. Van Nostrand Company, Inc., New York, 1935), p. 799.

[b] J. A. Victoreen, J. Appl. Phys. 20, 1141 (1949).

TABLE XIII. Xenon absorption coefficients from 80 - 202 Å.[a]

λ(Å)	k(cm^{-1})	λ(Å)	k(cm^{-1})
80.0	61	164.4	216
83.6	68	166.3	203
85.4	89	168.3	200
90.3	175	171.1	152
91.4	182	172.3	141
96.6	252	173.5	129
97.3	253	178.0	127
99.5	269	181.1	120
101.0	403	182.0	114
105.0	460	182.6	114
106.7	460	184.0	95
110.0	568	185.8	93
116.5	730	192.9	61
138.0	676	194.9	60
139.2	622	195.9	60
140.3	527	200.8	60
145.0	483	202.3	58
145.3	416	203.9	59
147.5	446	207.9	53
149.8	412	209.0	58
151.5	410	213.0	67
154.0	294	214.2	55
156.2	329	215.1	52
158.9	294	220.0	66
162.4	273		

[a] D. L. Ederer and D. H. Tomboulian, private communication.

TABLE XI. Xenon absorption coefficients from threshold to 280 Å.[a]

λ(Å)	k(cm^{-1})	λ(Å)	k(cm^{-1})	λ(Å)	k(cm^{-1})	λ(Å)	k(cm^{-1})
284.0	78	473.1	336	646.1	1006	870.1	1633
294.9	114	477.4	351	650.8	1025	880.3	1664
298.7	96	482.0	365	661.8	1055	888.0	1661
309.0	149	488.9	359	665.9	1099	902.5	1656
318.7	153	493.8	394	672.6	1109	906.3	1671
324.1	129	497.8	367	677.2	1090	911.6	1674
330.2	98	502.7	434	686.3	1150	920.6	1684
338.7	94	506.8	443	696.2	1201	924.3	1443
352.8	124	510.3	463	701.7	1189	924.9	1392
358.3	181	515.4	486	710.4	1238	928.8	1129
364.5	147	521.0	514.	715.6	1250	935.2	1622
369.0	189	528.1	537	722.1	1279	938.5	1695
376.1	150	534.2	558	726.3	1277	941.6	1326
382.6	178	540.7	594	738.5	1296	943.5	1929
390.7	185	546.3	[illegible]	746.8	1298	946.9	883
394.2	217	552.9	661	756.4	1371	951.9	2466
397.5	202	557.1	667	762.2	1385	955.9	629
400.5	198	560.4	620	769.1	1395	959.6	1318
405.7	169	566.3	684	776.3	1415	964.4	2416
410.6	185	572.4	627	781.6	1387	969.5	1966
416.6	194	588.0	818	784.9	1474	975.0	650
423.4	214	590.4	759	796.4	1462	979.5	1121
425.8	210	595.6	283	802.3	1482	983.1	1466
429.9	236	595.7	800	805.1	1488	988.1	2240
436.6	253	597.8	819	823.0	1463	991.6	2495
442.8	246	611.5	890	828.5	1530	996.1	3370
447.5	260	620.5	921	836.0	1525	1003.5	413
451.2	270	626.8	932	845.7	1540	1008.5	420
461.3	294	631.7	945	851.5	1561	1015.6	782
463.6	299	638.6	971	858.7	1614	1018.5	937
466.6	302	642.8	994	865.2	1607		

[a] Present data.

IV. DISCUSSIONS

1. Critical Absorption Energies

The critical absorption energy of an atom is the energy required to remove an electron from a given shell within the atom to infinity with zero kinetic energy. That is, it is an ionization potential of the atom. For the outer electrons these ionization potentials can be determined very accurately by spectroscopic means. However, for inner shell electrons and especially K-shell electrons the resonance absorption lines preceding the ionization limit may overlap one another and with the main absorption edge. Thus, it may or may not be possible to observe the true absorption edge and, in fact, many of the reported x-ray critical absorption energies actually represent minimum excitation energies.

If we know the binding energy of the electron in the first excited state of the atom we can determine the true absorption edge by subtracting this binding energy from the observed critical absorption energy. An approximate method for finding the binding energies for s-electrons in the rare gases is given in the next section.

Table XV presents the known critical absorption energies for the rare gases. There is still a lack of experimental data for some absorption edges, thus, the semi-empirical values given by R. D. Hill et al.[56] are also listed. These values are actually interpolated values obtained after revising the critical x-ray energies tabulated by M. Siegbahn.[58] The values quoted by Hill have been converted back into angstrom units

TABLE XV. Critical absorption energies of the rare gases expressed in angstrom units of wavelength.

Edge	He		Ne		Ar		Kr		Xe	
	Exp.	Theo.	Exp.	Calc.[d]	Exp.	Calc.[d]	Exp.	Calc.[d]	Exp.	Calc.[d]
K	504.26[a]	504.26[b]	14.298[c]	14.20	3.87147[c]	3.87	0.86555[c]	0.8657	0.3585[c]	0.3588
L										
1			255.77[e]	---	---	43.0	6.5107[c]	6.46	2.2737[c]	2.27
2			572.37[e]	---	50.1880[c]	50.0	7.1822[c]	7.14	2.4307[c]	2.43
3			574.93[e]	---	50.5977[c]	51.0	7.4009[c]	7.42	2.5929[c]	2.59
M										
1					424.03[e]	---	---	43.0	---	10.9
2					777.96[e]	---	56.3475[c]	58.0	13.1737[c]	12.5
3					786.72[e]	---	58.7509[c]	59.0		13.3
4							130.45[f]	130.0	---	18.1
5							132.14[f]		---	18.4
N										
1							450.62[e]	---	---	50
2							845.42[e]	---	89.183[c]	80
3							885.62[e]	---		83
4									178.33[f]	188
5									183.55[f]	191
O										
1									529.92[e]	---
2									922.75[e]	---
3									1022.14[e]	---

[a] G.Herzberg, Proc. Roy. Soc.(London) 248, 309 (1958). The actual value quoted is IP(H_e) = 198 310.82±.15 cm^{-1}.

[b] S.Chandrasekhar and G.Herzberg, Phys. Rev. 98, 1050 (1955). The actual value quoted is 198 310.4± 2 cm^{-1}.

[c] Y.Cauchois, J. Phys. Radium 16, 253 (1955). For the $M_{4,5}$ edge of Kr she quotes 142.488 Å.

[d] R.D. Hill, E.L. Church, and J.W. Mihelich, Rev. Sci. Instr. 23, 523 (1952).

[e] C.E. Moore, Atomic Energy Levels Circ. 467, Nat. Bur. Std. (U. S. Government Printing Office, Washington, D. C.), Vol. 1, (1949); Vol. 2, (1952); Vol. 3 (1958).

[f] K.Codling and R.P. Madden, Phys. Rev. Letters 12, 106 (1964).

using the same conversion factor of 1eV = 12396.44 x 10^{-8}. X-ray absorption energies are usually measured in x-ray units (xu) which are based on the lattice spacing of Na Cl. At present these x units are 0.202% smaller than the angstrom unit of length (10^{-8}cm). The critical absorption energies for the outer shell electrons were obtained from optical data.

2. Autoionized Energy Levels

The first absorption spectra of the rare gases in the vicinity of their ionization continua were obtained by Beutler[39] in 1935. He observed a series of diffuse absorption lines between the $M_{2,3}$, $N_{2,3}$, and $O_{2,3}$ edges in A, Kr, and Xe, respectively. These absorption lines appeared at higher energies than the first ionization potentials of the atoms. The interaction between these discrete levels and the underlying ionization continuum caused the levels to broaden considerably. In general, a radiationless transition takes place from the discrete levels into the continuum accompanied with the ejection of an electron. When this occurs the states are known as autoionized states. Measurements of the ionization yields within these diffuse states have been made by two methods. One by the direct use of a thermopile to measure the absolute intensity of the ionizing radiation and the other by measuring the yield relative to that of another rare gas. In each case the yield was found to be 100%. Figures 9, 10 and 11 illustrate these Beutler lines in Xe, Kr, and A, respectively, as obtained by Huffman et al. using photoelectric absorption techniques.

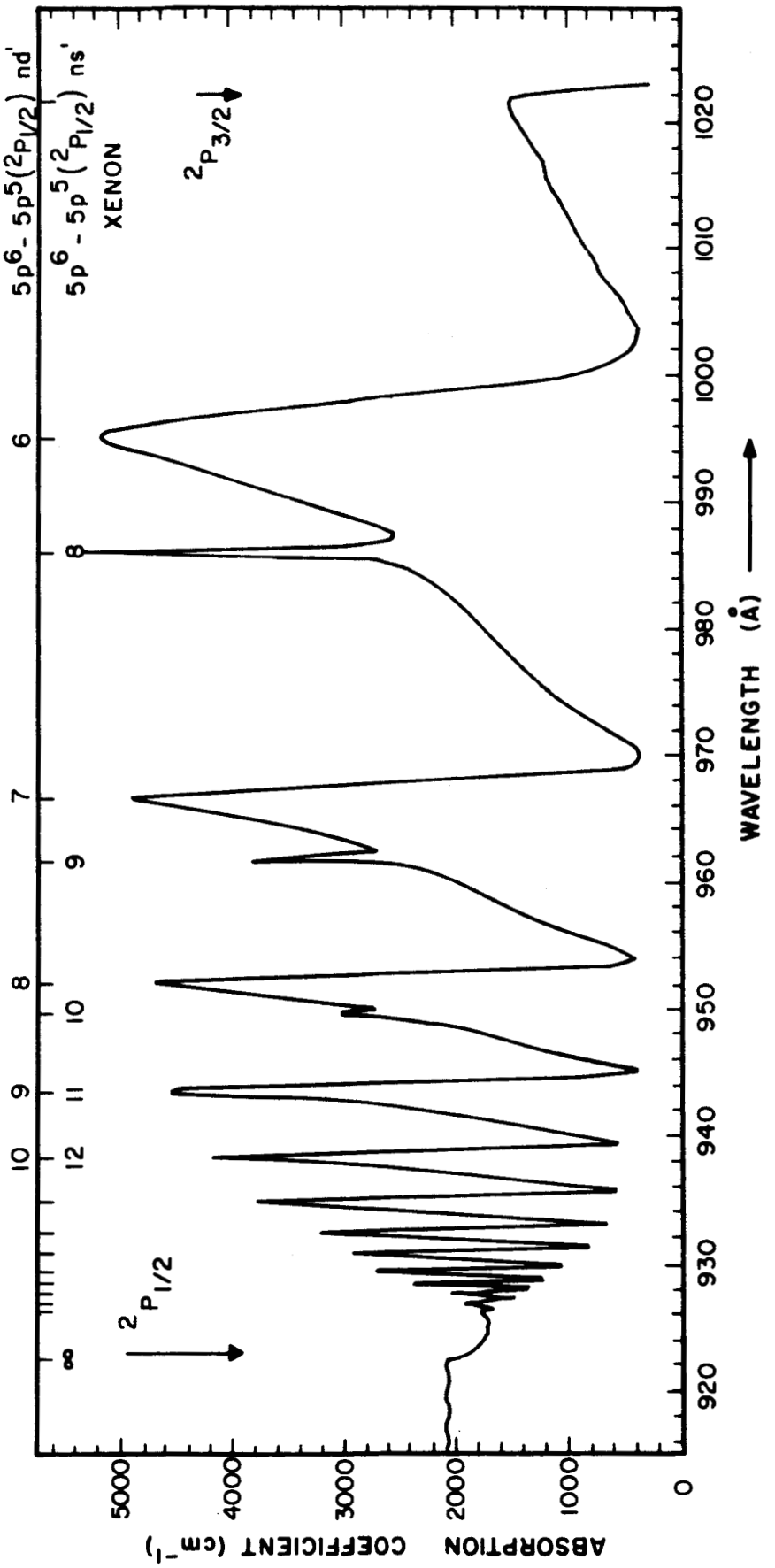

Figure 9. Beutler autoionized lines of xenon as measured by Huffman, et al. (ref. 36).

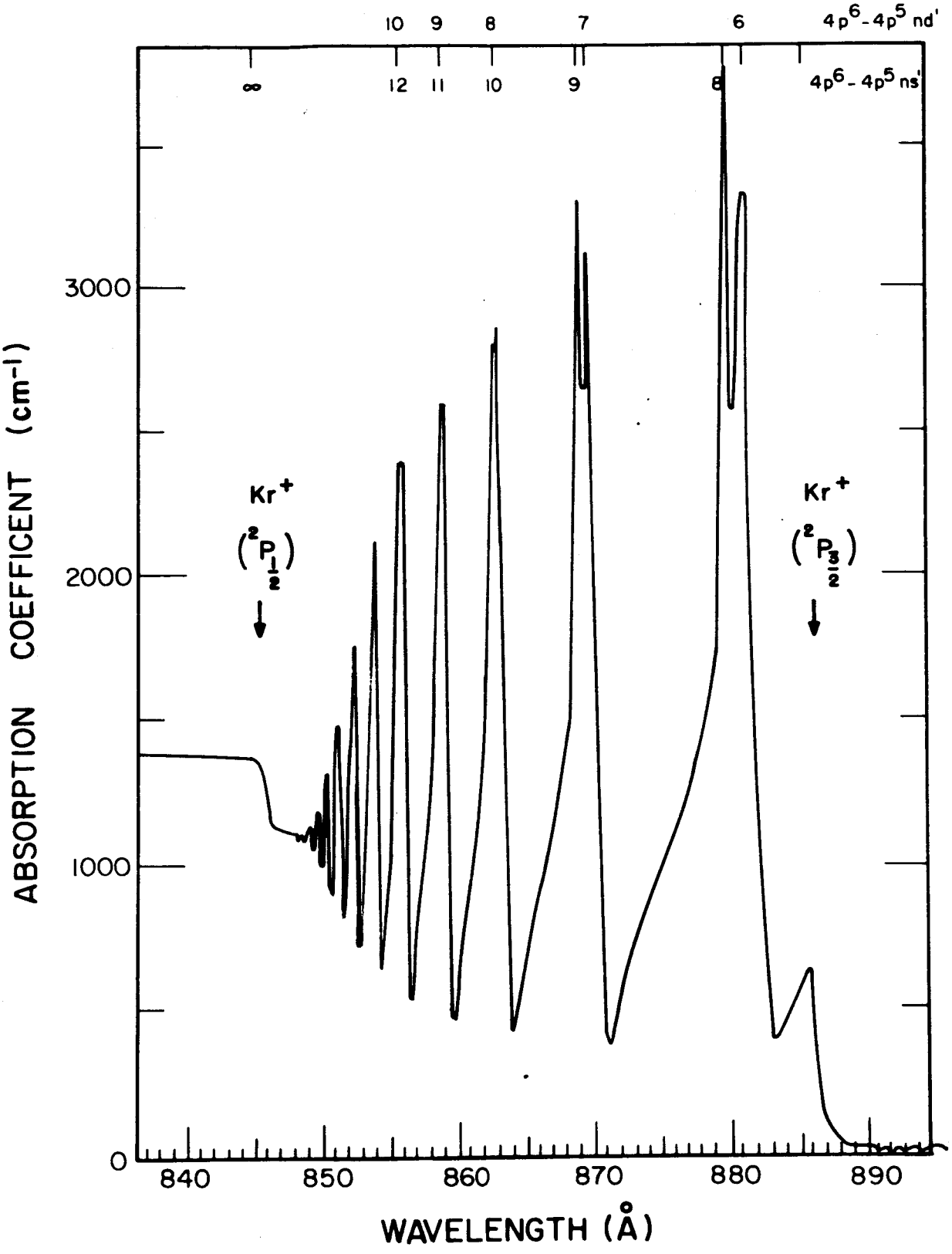

Figure 10. Beutler autoionized lines of krypton as measured by Huffman, et al. (ref. 54)

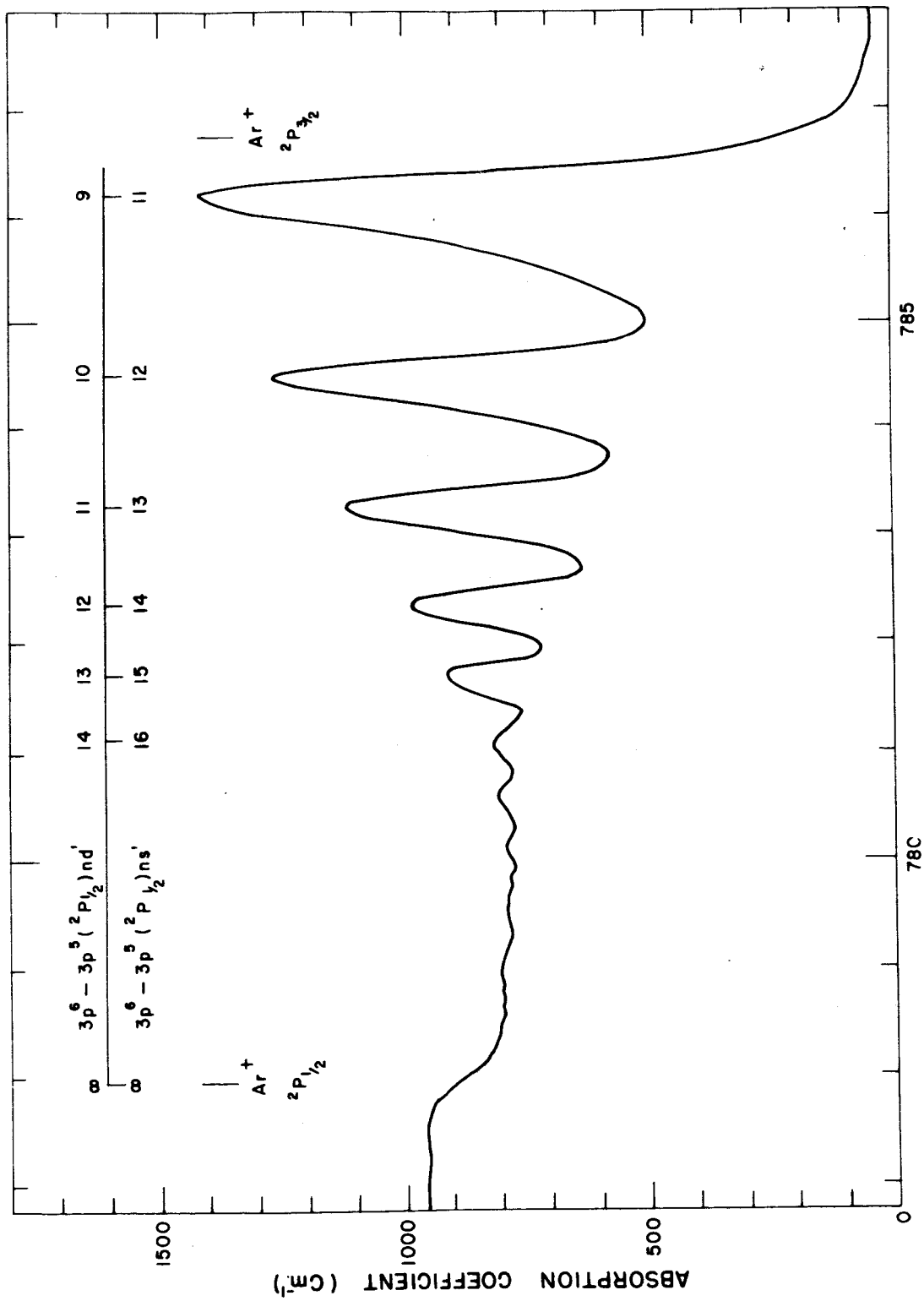

Figure 11. Beutler autoionized lines of argon as measured by Huffman et al. (Reference 36)

Beutler looked for absorption lines associated with the removal of inner s-electrons without success. Since he used the molecular helium continuum which provided useful radiation only down to 600 Å he concluded that if absorption lines exist they must appear at wavelengths below 600 Å. It was not until 1963, however, when utilizing the continuous radiation from a 180 Mev synchrotron that Madden and Codling first observed the absorption spectra of the rare gases below 600 Å.[2] Concurrent work on the total absorption cross sections of the rare gases using a densely populated line emission light source and a continuum provided by a flash tube also revealed absorption structure between 400 and 600 Å.[4,5,38,59] These can be seen in Figs. 12 and 13. It was shown that the position of these absorption lines could be predicted on the basis of the similarity between the electron configuration of the rare gases and the alkali metals.[5]

The predicted absorption energies were determined as follows: Consider the 5s-np transitions in Xe and 6s-np transitions in Cs. In both cases the electrons excited into the vacant p-shells see an atomic core of charge z = 1 surrounded by a completed sub-shell of six p-electrons. It is assumed that the excited electrons in the np shells of Cs are bound to their core with the same energies required for electrons in the np shells of Xe. The binding energies for the np electrons in Cs are readily found from known spectroscopic term values. Table XVI lists the binding energies for the np shells in Cs along with those for Na, Kr, and Rb. Equating these energies to the np shells in the rare gases and subtracting them from the ionization potentials of the s-electrons

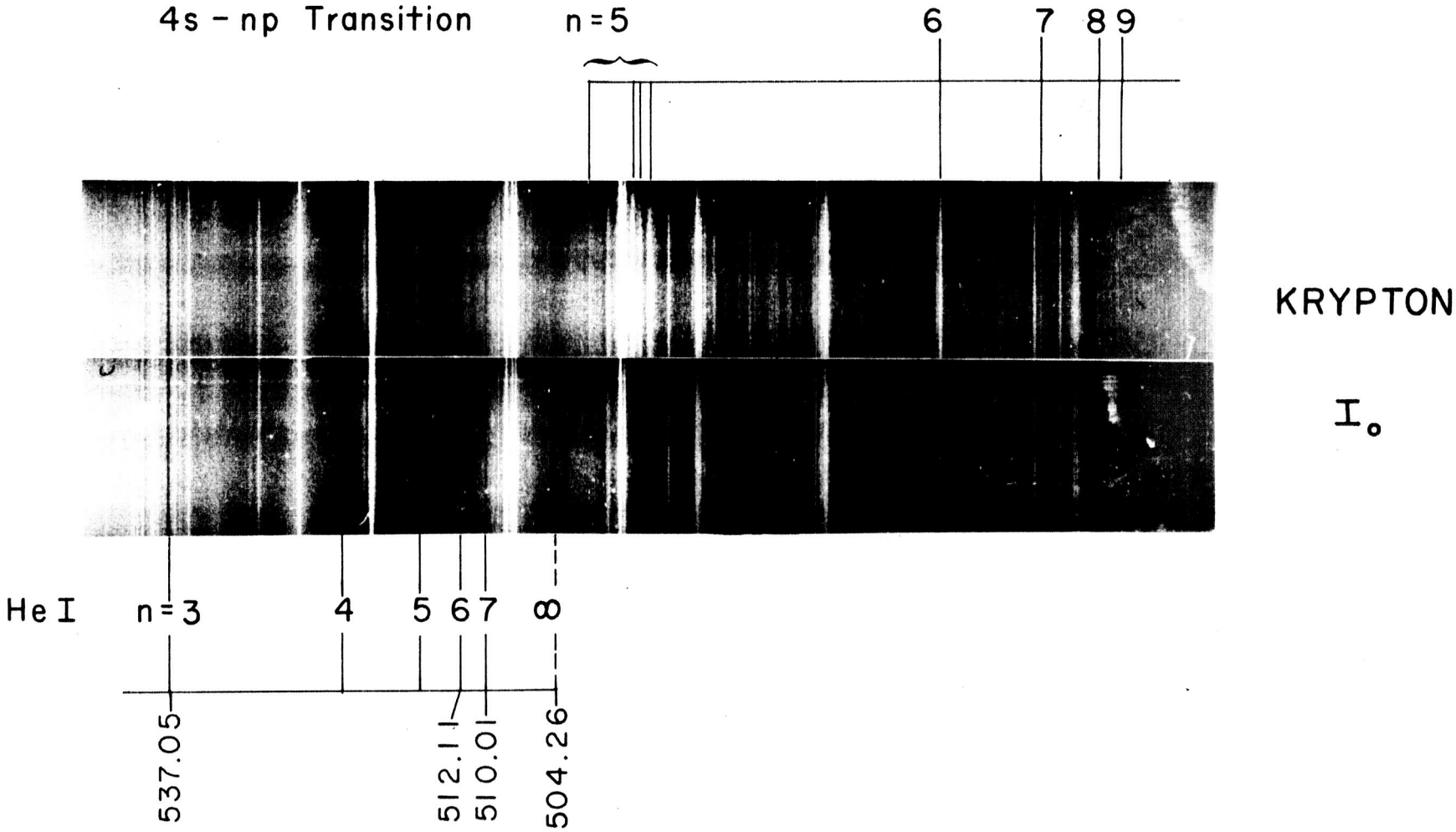

Figure 12. Absorption spectrum of Kr in the vicinity of its N_1 edge. The comparison spectrum I_o was taken before Kr was introduced into the spectrograph. The white lines common to both exposures represent discrete emission lines from the flash tube, while the marked white lines represent discrete windows in the absorption continuum. The helium self-absorption lines are expressed in angstroms.

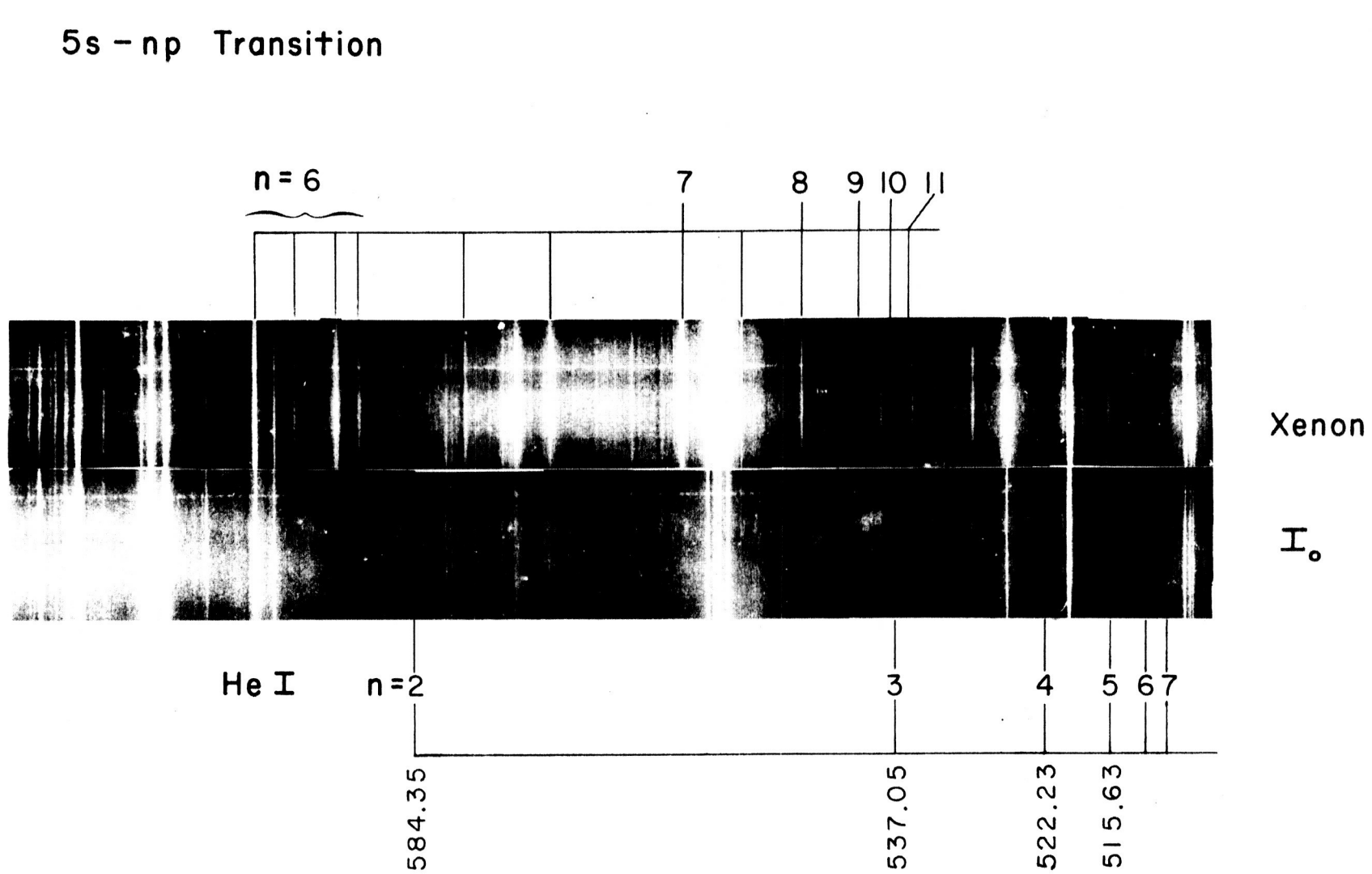

Figure 13. Absorption spectrum of Xe in the vicinity of its O_1 edge. The comparison spectrum I_o was taken before Xe was introduced into the spectrograph. As in Figure 12 the marked white lines indicate the discrete windows in absorption.

TABLE XVI. Binding energies for the valence electron in excited p-shells of the alkali metals. [a]

Desig.	Binding Energies (cm^{-1}) Sodium	Potassium	Rubidium	Cesium
3p	24 493.47			
4p	11 182.77	22 024.61		
5p	6 409.38	10 308.34	21 112.06	
6p	4 153.14	6 010.49	9 975.83	20 228.47
7p	2 909.25	3 939.80	5 855.97	9 641.06
8p	2 151.11	2 782.36	3 856.06	5 697.57
9p	1 655.12	2 069.44	2 732.08	3 769.42
10p	1 312.42	1 599.44	2 037.14	2 679.62

[a] Obtained from optical term values, C. E. Moore, Atomic Energy Levels, Circ. 467, Nat. Bur. Std. (U. S. Government Printing Office, Washington, D. C.), Vol. 1, (1949); Vol. 2, (1952); Vol. 3, (1958).

the position of the ms-np absorption series can be found. Table XVII compares the observed and predicted absorption spectra. The first observed absorption line in Kr and Xe appear to be split into four levels which is compatible with LS or jj coupling, however, in the case of Kr the absorption spectrum obtained by Madden and Codling clearly show only three levels, the line at 501.11 Å being absent. It would appear, therefore, that the 501.11 Å line is caused by an impurity. The first two predicted lines in Kr and Xe were obtained by using J = 1/2 and 3/2 when determining the binding energies, all other predicted values were found for J = 1/2.

This method for predicting the absorption series of a rare gas can be applied to absorption due to the more tightly bound electrons. In fact, it was applied to argon as early as 1926 by Coster and Van der Tuuk[60] to explain the fine structure in the vicinity of the K absorption edge. Parrat,[61] in 1939, obtained a more highly resolved K absorption spectrum in argon which clearly resolved the first two members of the 1s-np series ($n \geqslant 4$). Using the binding energies for the np shells of potassium and the observed wavelengths of the argon absorption lines he placed the main absorption edge (i.e., the K ionization potential) at a wavelength position some 4 xu less than its usually accepted measured value.

The K absorption spectrum for Kr has been measured by Shaw (1940).[62] No discrete structure due to 1s-np type transitions was observed. It is possible that the discrete structure cannot be resolved due to their natural width overlapping with each other and with the K edge.

TABLE XVII. Observed and predicted absorption spectra due to excitations of the type ms-np in the rare gases. Wavelengths are expressed in angstroms.

	Ne 2s-np		Ar 3s-np		Kr 4s-np		Xe 5s-np	
n	Pred.[a]	Obs.[b]	Pred.[a]	Obs.[b]	Pred.[a]	Obs.[c]	Pred.[a]	Obs.[c]
3	272.9	272.6						
4	263.3	263.2	467.7	466.3				
5	260.0	259.9	443.4	443.1	498.0 497.4	501.11 497.46 496.87 496.04		
6	258.5	258.5	435.1	435.0	471.8	471.54	593.5 591.6	599.95 595.92 591.81 589.62
7	257.7	257.7	431.2	431.2	462.8	462.75	558.2	557.92
8	257.2	257.1	429.1	428.9	458.6	457.85	546.5	546.16
9	256.9	---	427.8	427.6	456.2	456.14	540.7	540.71
10	256.6	---	426.9	426.7	454.8	---	537.6	537.40
11	256.4	---	426.3	---	453.8	---	535.6	535.62
Series Limit[a]	255.77		424.03		450.62		529.92	

[a] Energy levels used in the calculations were obtained from C.E. Moore, Atomic Energy Levels, Circ. Nat. Bur. Std. 467, Vol. I (1949); Vol. II (1952); Vol. III (1958).

[b] R. Madden and K. Codling, Phys. Rev. Letters, 10, 516 (1963).

[c] J.A.R. Samson, Physics Letters (January, 1964)

V. SUMMARY

The photoionization cross sections of the rare gases have been measured from their ionization thresholds to 280 Å. Published and unpublished data have been compiled and tabulated. In the case of He, Ne, and A the tabulated data essentially provide absorption coefficients continuously from threshold to .01 Å. Although continuous data for the K-shell is tabulated down to .01 Å for Kr and Xe there is very little information available for the remaining inner shells. Figure 14 summarizes the photoionization cross sections of the rare gases as a function of wavelength. The vertical lines indicate the positions of the "window" type discrete absorption lines.

On the whole, very little theoretical work has been performed on photoionization cross sections of the rare gases. Helium has been studied thoroughly and the theoretical results are in excellent agreement with experiment. The theoretical results of neon are in fair agreement with experiment. In the case of argon and krypton only order of magnitude agreement is obtained, while no theoretical treatment of xenon has yet been attempted. Figure 15 shows the absorption coefficients of the rare gases plotted as a function of energy above the $^2P_{\frac{1}{2}}$ threshold. This is perhaps a more convenient plot for comparison with theoretical results. It is of interest to point out that the curves for A, Kr, and Xe all intersect at one point approximately 6eV

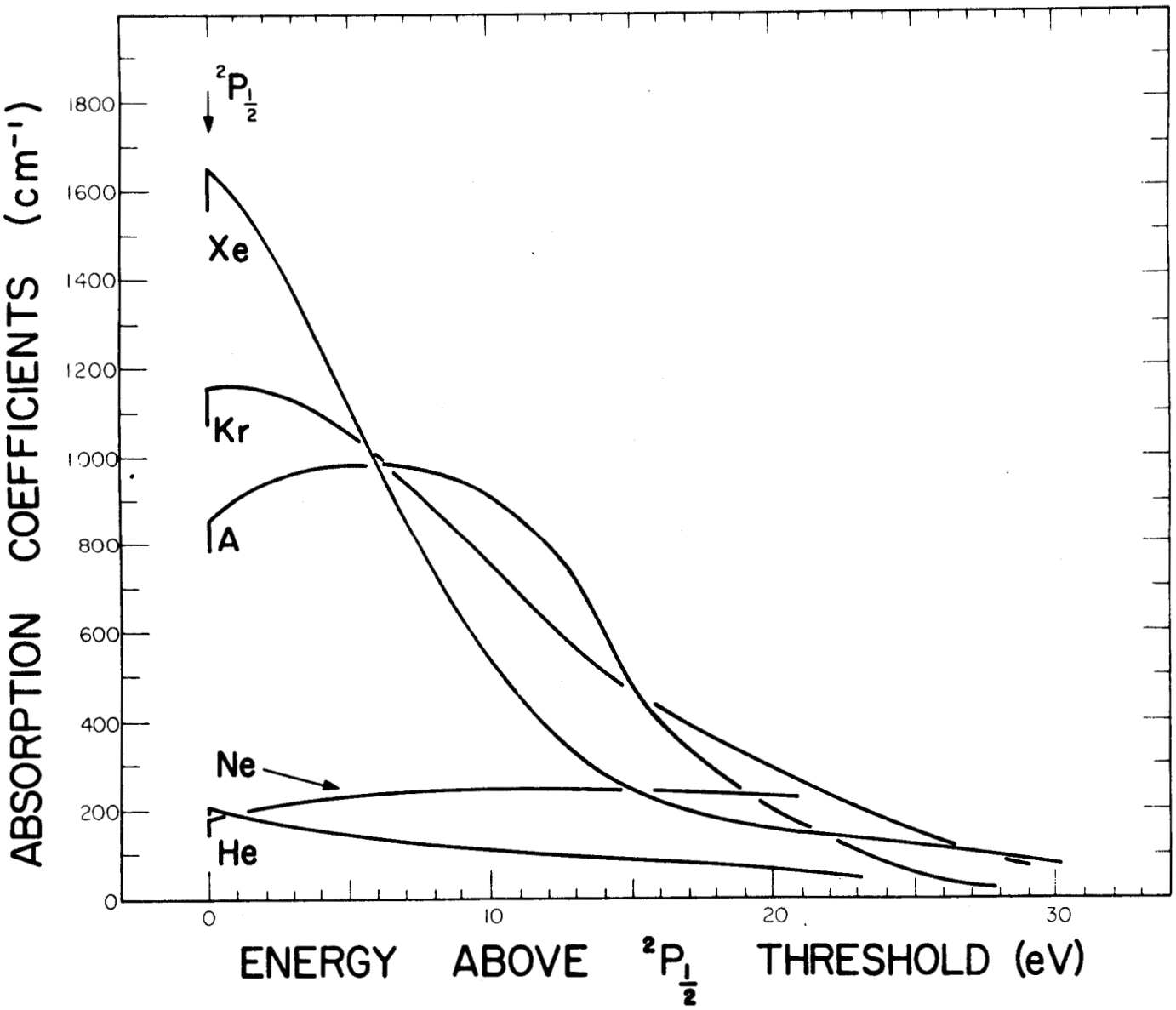

Figure 14. Photoionization continuum cross sections of the rare gases as a function of wavelength. The vertical lines indicate the positions of the discrete "window" type absorption lines in A, Kr, and Xe due to (ms-np) type transitions.

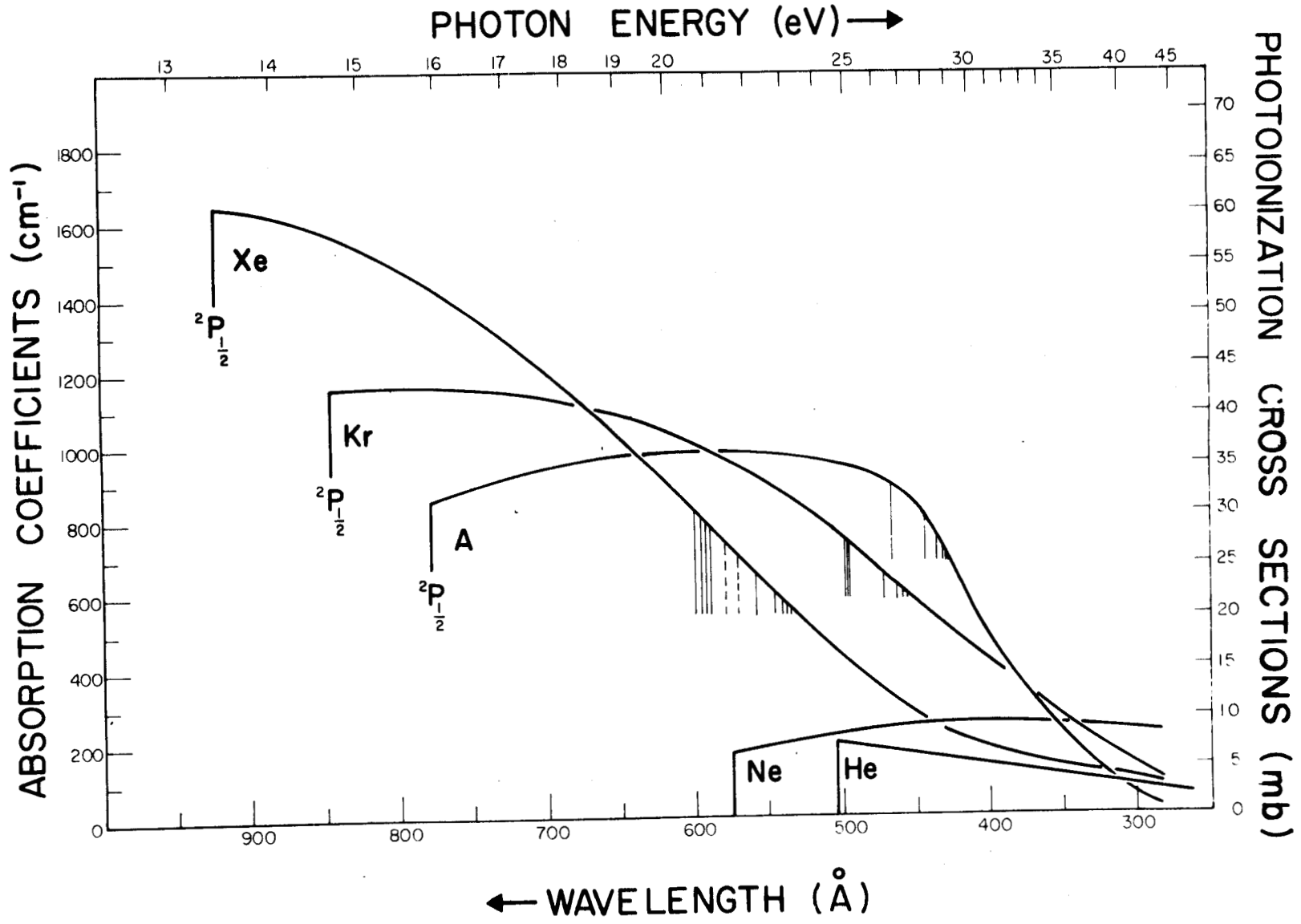

Figure 15. Photoionization absorption coefficients vs energy above the $^2P_{\frac{1}{2}}$ threshold.

above the $^2P_{\frac{1}{2}}$ threshold.

The position of previously unknown discrete absorption structure overlying the ionization continuum has been sought and, in many cases, found. Over and above their importance to atomic structure it is desirable to know the position of the discrete lines since these are regions to be avoided if possible when using the rare gases in ion chambers for absolute intensity measurements of vacuum ultraviolet radiation.

The oscillator strengths for excitations into the photoionization continuum have been discussed. It has been shown, in the case of helium, that knowledge of the total continuum oscillator strength in conjunction with the Thomas-Kuhn sum rule provides immediately the total discrete f-numbers. For this approach, however, it is necessary to know the values of the absorption coefficients to a high degree of accuracy. For helium an uncertainty of $\pm$ 5% in the value of the absorption coefficients will give an uncertainty of $\pm$ 17% in the value of the total discrete f-number.

A summary of the continuum f-numbers shell by shell is given in Table XVIII. For the K-shells the f-numbers were evaluated down to .01 Å. The contributions to the outermost shells include the f-numbers of the Beutler lines.

TABLE XVIII. Summary of the continuum oscillator strengths for the rare gases.

Gas	Continuum f-numbers K[b]	L	M	N	O	Theoretical total=Z f (continuum + line)
He	1.54					2
Ne	1.81	8.22				10
A	1.77	7.51	5.69[a]			18
Kr	1.63	---	---	6.3		36
Xe	1.57	---	---	---	6.01	54

[a] This value was obtained by extrapolating data from 280-50 Å. There is some theoretical evidence that the k value may increase in this region, hence the f-number will also increase.

[b] The continuum f-numbers for the K shell were measured down to .01 Å.

REFERENCES

1. J.A.R. Samson, J. Opt. Soc. Am. 54, 6 (1964).
2. R.P. Madden and K. Codling, Phys. Rev. Letters 10, 516 (1963).
3. R.P. Madden and K. Codling, J. Opt. Soc. Am. (Feb. 1964).
4. J.A.R. Samson, Phys. Rev. 132, 2122 (1963).
5. J.A.R. Samson, Physics Letters 8, (Jan. 1964).
6. L.B. Loeb, Basic Process of Gaseous Electronics, (University of California Press, Berkeley, 1955), p. 651.
7. J.P. Vinti, Phys. Rev. 44, 524 (1933).
8. J.A. Wheeler, Phys. Rev. 43, 258 (1933).
9. H. Köwien, Z. Physik 91, 1 (1934).
10. S. Huang, Astrophys. J. 108, 354 (1948).
11. A. Dalgarno and N. Lynn, Proc. Phys. Soc. 70, 802 (1957).
12. A. Dalgarno and A.L. Stewart, Proc. Phys. Soc. 76, 49 (1960).
13. E.E. Salpeter and M.H. Zaidi, Phys. Rev. 125, 248 (1962).
14. A.L. Stewart and W.J. Wilkinson, Proc. Phys. Soc. 75, 796 (1960).
15. A.L. Stewart and T.G. Webb, Proc. Phys. Soc. 82, 532 (1963).
16. J.W. Cooper, Phys. Rev. 128, 681 (1962).
17. Po Lee and G.L. Weissler, Phys. Rev. 99, 540 (1955).
18. N. Axelrod and M.P. Givens, Phys. Rev. 115, 97 (1959).
19. D.J. Baker, D.E. Bedo, and D.H. Tomboulian, Phys. Rev. 124, 1471 (1961).
20. J.F. Lowry and D.H. Tomboulian, Tech. Rep. No. 3, ARO(D) Project No. 2810P, (Sept. 1963).
21. J.P. Vinti, Phys. Rev. 42, 632 (1932).
22. E.A. Hylleraas, Z. Physik 106, 395 (1937).

23. E. Trefftz, A. Schulter, K.H. Dettmar, and K. Jorgens, Z. Astrophysik 44, 1 (1957).

24. J. Hargreaves, Proc. Camb. Phil. Soc. 25, 91 (1928-29).

25. D.R. Bates, Mon. Not. R. Astr. Soc. 100, 25 (1939).

26. Po Lee and G.L. Weissler, J. Opt. Soc. Am. 42, 214 (1952); Proc. Roy. Soc. (London) 219, 71 (1953).

27. R.W. Ditchburn, Proc. Phys. Soc. 75, 461 (1960).

28. M.J. Seaton, Proc. Roy. Soc. (London) 208, 408 (1951); Proc. Phys. Soc. A67, 927 (1954).

29. D.L. Ederer and D.H. Tomboulian, Tech. Rep. No. 10, Contract No. Nonr-401(37), (June 1963).

30. A. Gold and R.S. Knox, Phys. Rev. 113, 834 (1959).

31. H.H. Landolt and R. Börnstein, Zahlenwerte und Funktionen (Springer-Verlag, Berlin, 1950), sixty edition, Vol. 1, Part 1, p. 264.

32. N. Wainfan, W.C. Walker, and G.L. Weissler, Phys. Rev. 99, 542 (1955).

33. Po Lee and G.L. Weissler, Phys. Rev. 99, 540 (1955).

34. P.H. Metzger and G.R. Cook, Aerospace Corp., Calif., (private communication).

35. R.E. Huffman, Y. Tanaka, and J.C. Larrabee, J. Chem. Phys. 39, 902 (1963).

36. D.H. Tomboulian and D.L. Ederer, Cornell University, Ithaca, N. Y. (private communication).

37. O P. Rustgi, J. Opt. Soc. Am. (to be published).

38. J.A.R. Samson, J. Opt. Soc. Am. (March 1964).

39. H. Beutler, Z. Physik 93, 177 (1935).

40. A. Dalgarno, Proc. Phys. Soc. (London) 65, 663 (1952).

41. A. Dalgarno, Queen's University, Belfast, (private communication).

42. J. Wheaton and W.R.S. Garton, Imperial College, London, (private communication).

43. U. Fano, Phys. Rev. 124, 1866 (1961).

44. G.L. Weissler, J.A.R. Samson, M. Ogawa, and G.L. Cook, J. Opt. Soc. Am. 49, 338 (1959).

45. J.A.R. Samson, Thesis, University of S. California (1958).

46. E. Schönheit, Z. Naturforsch. 16a, 1094 (1961).

47. F. Comes and W. Lessman, Z. Naturforsch. 16a, 1396 (1961).

48. S.J.M. Allen, as compiled in A.H. Compton and S.K. Allison, X-Rays in Theory and Experiment, (D. Van Nostrand Company, Inc., New York, 1935), p. 799.

49. B.L. Henke, J. Appl. Phys. 28, 98 (1957).

50. J.A. Victoreen, J. Appl. Phys. 20, 1141 (1949).

51. R.S. Knox, Phys. Rev. 110, 375 (1958).

52. K. Codling and R.P. Madden, Phys. Rev. Letters 12, 106 (1964).

53. A. Pery-Thorne and W.R.S. Garton, Proc. Phys. Soc. (London) 76, 833 (1960).

54. R.E. Huffman, Y. Tanaka, and J.C. Larabee, Appl. Opt. 2, 947 (1963).

55. O.P. Rustgi, E.I. Fisher, and C.H. Fuller, J. Opt. Soc. Am. (to be published).

56. R.D. Hill, E.L. Church, and J.W. Mihelich, Rev. Sci. Instr. 23, 523 (1952).

57. D. Anderson and W. Lichten, Bull. Am. Phys. Soc. 9, 65 (1964).

58. M. Siegbahn, Spektroskopie der Rontgenstrahlen (Verlag Julius Springer, Berlin, 1931), second edition, pp. 346-349.

59. J.A.R. Samson, J. Opt. Soc. Am. (to be published).

60. Coster and Van der Tuuk, Z. Physik 37, 367 (1926).

61. L.G. Parratt, Phys. Rev. 56, 295 (1939).

62. C.H. Shaw, Phys. Rev. 57, 877 (1940).